SANDIA REPORT
SAND2000-0715
Unlimited Release
Printed March 2000

New Methods for Predicting Lifetimes, Part 2: The Wear-out Approach for Predicting the Remaining Lifetime of Materials

Kenneth T. Gillen and Mat Celina

Prepared by
Sandia National Laboratories
Albuquerque, New Mexico 87185 and Livermore, California 94550

Sandia is a multiprogram laboratory operated by Sandia Corporation, a Lockheed Martin Company, for the United States Department of Energy under Contract DE-AC04-94AL85000.

Sandia National Laboratories

Issued by Sandia National Laboratories, operated for the United States Department of Energy by Sandia Corporation.

Available to DOE and DOE contractors from
Office of Scientific and Technical Information
P.O. Box 62
Oak Ridge, TN 37831

Prices available from (703) 605-6000
Web site: http://www.ntis.gov/ordering.htm

Available to the public from
National Technical Information Service
U.S. Department of Commerce
5285 Port Royal Rd
Springfield, VA 22161

SAND2000-0715
Unlimited Release
Printed March 2000

New Methods for Predicting Lifetimes. Part 2- The Wear-out Approach for Predicting the Remaining Lifetime of Materials

Kenneth T. Gillen and Mat Celina
Organic Materials Aging and Reliability Department
Sandia National Laboratories
P.O. Box 5800
Albuquerque, NM 87185-1407

ABSTRACT

The so-called Palmgren-Miner concept that degradation is cumulative, and that failure is therefore considered to be the direct result of the accumulation of damage with time, has been known for decades. Cumulative damage models based on this concept have been derived and used mainly for fatigue life predictions for metals and composite materials. We review the principles underlying such models and suggest ways in which they may be best applied to polymeric materials in temperature environments. We first consider cases where polymer degradation data can be rigorously time-temperature superposed over a given temperature range. For a step change in temperature after damage has occurred at an initial temperature in this range, we show that the remaining lifetime at the second temperature should be linearly related to the aging time prior to the step. This predicted linearity implies that it may be possible to estimate the remaining lifetime of polymeric materials aging under application ambient conditions by completing the aging at an accelerated temperature. We refer to this generic temperature-step method as the "Wear-out" approach. We then outline the expectations for Wear-out experiments when time-temperature superposition is invalid, specifically describing the two cases where so-called "interaction effects" are absent and are present. Finally, we present some preliminary results outlining the application of the Wear-out approach to polymers. In analyzing the experimental Wear-out results, we introduce a procedure that we refer to as time-damage superposition. This procedure not only utilizes all of the experimental data instead of a single point from each data set, but also allows us to determine the importance of any "interaction effects".

ACKNOWLEDGEMENTS

The authors gratefully acknowledge able experimental assistance from G. M. Malone (elongation, density and modulus measurements), J. Wise (oxygen consumption experiments) and A. C. Graham (oxygen consumption and density measurements).

CONTENTS

INTRODUCTION 1
EXPERIMENTAL 1
- Materials 1
- Oven Aging 2
- Tensile Tests 2
- Oxygen consumption measurements 2
- Density measurements 2

RESULTS AND DISCUSSION 3
- Accelerated aging and time-temperature superposition 3
- Diffusion-limited oxidation 6
- Wear-out approach for predicting remaining lifetime 7
- Applying the Wear-out approach to experimental EPDM results 11
- Applying the Wear-out approach to Surveillance EPDM o-rings 13

REFERENCES 17

TABLE

1 SR793B-80 formulation 2

FIGURES

1 Oxygen consumption rate data for several materials 18
2 Oxygen consumption rates for nitrile rubber material 18
3 Oxygen consumption rates for neoprene rubber material 19
4 Normalized elongation results for the nitrile rubber material 19
5 Normalized elongation results for the neoprene rubber material 20
6 Normalized elongation results for the CSPE rubber material 20
7 Time-temperature superposition of the nitrile data from Fig. 4 21
8 Time-temperature superposition of the neoprene data from Fig. 5 21
9 Time-temperature superposition of the CSPE data from Fig. 6 22
10 Arrhenius plot of nitrile rubber shift factors 22
11 Arrhenius plot of neoprene and CSPE elongation shift factors 23
12 Modulus profile results for the nitrile rubber material 24
13 Representative relationship between degradation and lifetime 25
14 Superposed nitrile elongation results versus fractional lifetime 25
15 Hypothetical Wear-out plots 26
16 Hypothetical example of a non-superposable degradation property 26
17 Hypothetical Wear-out experiment for Fig. 16 data (no interaction) 27
18 Hypothetical Wear-out experiment for Fig. 16 data (interaction) 27
19 Elongation results for the SR793B-80 material 28
20 Oxygen consumption results for the SR793B-80 material 28
21 Wear-out results for the SR793B-80 material for aging at 125°C 29
22 Wear-out results for the SR793B-80 material for aging at 111°C 29
23 Density results at 150°C for SR793B-80 previously aged at 125°C 30

24 Density results at 150°C for SR793B-80 previously aged at 111°C 30
25 Time-degradation superposition of the density results from Fig. 23 31
26 Time-degradation superposition of the density results from Fig. 24 31
27 Elongation results at 140°C for E529-60 EPDM 32
28 Density results at 140°C for new and 23 year-old E529-60 EPDM 32
29 Wear-out plot using the density results from Fig. 28 33
30 Time-temperature superposition of nitrile rubber density results 33
31 OIT results for polybutylene from reference 22 34
32 OIT results for polybutylene from reference 24 34
33 OIT results for XLPE and EPR from references 26 and 27 35

INTRODUCTION

Given the importance of predicting polymer lifetimes in critical applications (e.g., nuclear weapons, nuclear reactor safety components), considerable effort has been devoted to developing improved accelerated aging methods [1]. Most accelerated aging approaches first expose unaged material to various accelerated environments and then measure and model the changes that occur in the material. The goal is to extrapolate the accelerated results obtained in order to predict the material lifetime under ambient aging conditions. In the best situation, if material is available that has been ambiently aged for a significant period of time, the properties of this material can be used to check the extrapolated predictions.

In addition to this obvious application of ambiently aged material, it would be advantageous to have a methodology for using this resource to estimate the material's remaining lifetime in the ambient environment. For instance, EPDM o-rings have been in the field for more than twenty years on certain weapon systems. If sacrificial samples of these o-rings could be used to estimate their remaining lifetimes, then more confidence would exist in any accelerated aging prediction [1]. One promising technique, which we refer to as the "Wear-out" approach, is based on the well-established, so-called Palmgren-Miner concept that degradation is cumulative [2,3] and that failure is therefore considered to be the direct result of the accumulation of damage with time. In this report, we review the principles underlying this Wear-out approach and show how they can best be applied to polymeric materials in temperature environments. To fully appreciate the application of Wear-out methods to polymeric materials, we will first briefly review the important concepts of time-temperature superposition and diffusion-limited oxidation (DLO) effects.

EXPERIMENTAL

Materials

EPDM elastomers represent terpolymers of ethylene, propylene and a nonconjugated diene. Much of the work for the current study was done on compression-molded sheets (~150 mm by 150 mm by 2 mm) of a compound designated SR793B-80, an EPDM that was specially formulated for the Honeywell Kansas City Plant and is used for the environment seals on a current weapon system. Its formulation is summarized in Table 1. Nordel 1440 is a terpolymer of ethylene, propylene and 1,4 hexadiene, with an approximate ethylene to propylene ratio of 53 to 47 and approximately 3 pph of the hexadiene. Zipstick 85 is zinc oxide powder, DiCup 40C and SR-350 are co-curing agents (40% active dicumyl peroxide and trimethylol propane trimethacrylate, respectively) and Flectol H is an antioxidant (polymerized 1,2, dihydro-2,2-4-trimethyl quinoline). A second EPDM o-ring material was a commercial material obtained as o-rings from Parker Seal Co. It was designated as compound E629-60 and is a proprietary formulation that was used for the environmental seals on a retired weapon system.

Table 1. SR793B-80 Formulation.

Constituent	pph
DuPont Nordel 1440	100
Zipstick 85	5
N-990 carbon black	40
N-539 carbon black	25
Flectol H	2
DiCup 40C	12
SR-350	10

Oven aging

Oven aging of the compression molded sheet materials and the o-ring pieces was carried out in air-circulating ovens (±1°C) equipped with thermocouples connected to continuous strip chart recorders.

Tensile tests

Tensile samples (~150 mm long by 6 mm wide by ~2 mm thick) of the SR793B-80 material were cut from the compression molded sheets before aging. The E529-60 o-ring samples were cut and tensile tested in tubular form. Tensile testing (5.1 cm initial jaw separation, 12.7 cm/min strain rate) was performed on an Instron 1000 tensile testing machine equipped with pneumatic grips; an extensometer clamped on the sample allowed ultimate tensile elongation values to be obtained.

Oxygen consumption measurements

Oxygen consumption rates were measured using a technique that has been described in detail elsewhere [4]. This technique monitors the change in oxygen content caused by reaction with polymer in sealed containers using gas chromatographic detection.

Density measurements

Density measurements were made using the Archimedes approach [5-6], where the sample (typically 50 mg) is weighed in air and then in ethanol on a balance with a reproducibility of better than 10 micrograms. Each reported measurement represented the average of a minimum of 3 samples.

RESULTS AND DISCUSSION

Accelerated aging and the time-temperature superposition approach

The approach normally used to accelerate the oxidative aging of polymers is to raise the air-oven aging temperature, thereby increasing the rates of the oxidative reactions which often dominate the degradation. The reactions underlying oxidative degradation of elastomers can be extremely complex and usually have not been worked out in detail. Fortunately, variants [7] of the basic autoxidation scheme (BAS), derived many decades ago by Bolland [8], Bateman [9] and co-workers for the homogeneous oxidation of liquid hydrocarbons, have proved to offer reasonable approximations to the degradation of many polymers [4,10]. For illustrative purposes, we will use the simplified scheme shown below; it represents a first approximation for the oxidation of stabilized polymers containing antioxidants (AH).

$$\text{Polymer} \xrightarrow{k_1} \text{R}\bullet$$

$$\text{R}\bullet + \text{O}_2 \xrightarrow{k_2} \text{RO}_2\bullet$$

$$\text{RO}_2\bullet + \text{RH} \xrightarrow{k_3'} \text{RO}_2\text{H} + \text{R}\bullet$$

$$\text{RO}_2\text{H} \xrightarrow{k_4} 2\text{R}\bullet + \text{ROH} + \text{HOH}$$

$$\text{RO}_2\bullet \xrightarrow{k_5 = k_5'[\text{AH}]} \text{Products}$$

$$\text{R}\bullet \xrightarrow{k_6 = k_6'[\text{AH}]} \text{Products}$$

Analysis of this kinetic scheme under steady-state conditions for R•, RO_2• and RO_2H leads to

$$\frac{d[\text{O}_2]}{dt} = \frac{C_1[\text{O}_2]}{1 + C_2[\text{O}_2]} \tag{1}$$

where C_1 and C_2 are constants involving several of the kinetic rate constants [4,10].

The first important conclusion from the result shown in eq. (1) is that such kinetic analyses predict a constant rate of reaction under constant temperature conditions. This turns out to be a reasonable approximation for many stabilized polymers. As an example, Fig. 1 shows some representative isothermal oxygen consumption rate results versus aging time for the SR793B-80 EPDM [1] and two other important elastomers [11]. For this plot, the time coordinate for the aging of each material is normalized to the time necessary for the ultimate tensile elongation to reach 10% of its initial value, which we arbitrarily define as the material's mechanical lifetime. The results show that the oxygen consumption rate is relatively constant over the entire mechanical degradation lifetime (0 to 1.0 on the x-axis) for the neoprene and nitrile materials and reasonably constant for the SR793B-80 EPDM (this material shows a moderate drop at early times). After severe

mechanical degradation has been reached, the oxygen consumption rate does begin to increase for the neoprene and EPDM materials. This rise, however, is of little consequence to modeling lifetimes since it occurs after mechanical "failure".

When we change the temperature, the rate of degradation will change. But for approximately linear situations like those shown in Fig. 1, one might expect approximately linear behavior at other temperatures. Evidence [11] in support of this assumption is shown in Figs. 2 and 3 for the nitrile and neoprene materials (as noted above, the late increases for the neoprene occur after mechanical failure). A reasonable assumption in polymer aging is the expectation that an equivalent amount of oxidation at two different temperatures leads to equivalent mechanical damage. Given the multiplicative change in oxidation rates between these temperatures (Figs. 2 and 3), this implies that mechanical degradation curves at different constant temperatures should have approximately the same shape when plotted versus the log of the aging time. Results consistent with such expectations can be seen in Fig. 4, which shows normalized elongation results (elongation divided by the elongation for the unaged material) for the nitrile rubber material aged at five temperatures. Similar observations of approximately constant degradation shape have been found for many other materials. Examples include neoprene [12] and chlorosulfonated polyethylene [13] cable jacketing materials, whose normalized tensile elongation results are shown in Figs. 5 and 6, respectively.

The most common method of analyzing aging data, such as those shown in Fig. 4-6, involves first choosing some arbitrary failure criterion, for instance the time for the elongation to reach 25% of its initial value. The values of the failure time at each temperature can then be used to test various aging models. For instance, the commonly used Arrhenius model assumes that an activated chemical process with activation energy E_a determines the temperature dependence of k, the rate of degradation, i.e.

$$k \propto \exp\left(\frac{E_a}{RT}\right) \tag{2}$$

Determining whether a plot of the log of the failure time versus inverse absolute aging temperature yields linear results can serve as a test of this model. Unfortunately, the above procedure uses only one processed datum point from each curve, eliminating most of the experimental points from analysis. However, if a constant multiplicative factor relates each temperature pair, then the same functional relationship between time and temperature will hold regardless of where on the degradation curve one chooses to analyze. Thus, if the results give Arrhenius behavior at 25% of initial elongation, they should follow the same Arrhenius relationship at 50%, 75%, etc. (linear with the same slope).

A better approach to test for the presence of constant multiplicative factors and to determine the relationship between time and temperature involves the time-temperature superposition concept [10,14]. For this approach, we first select the lowest experimental

temperature (e.g., 64.5°C for the data shown in Fig. 4) as the reference temperature. Then, for each set of data at a higher temperature T, we multiply the experimental times at this temperature by a constant shift factor, a_T, chosen empirically to give the best overall superposition with the reference temperature data ($a_T = 1$ at the reference temperature). Figures 7-9 show the results of applying this procedure to the elongation data of Figs. 4-6, respectively. In these figures, the bottom x-axes give the superposed results at the reference temperature appropriate to each material. The excellent superposition that occurs is not surprising, given the earlier observation that, for each material, the raw experimental results at the various temperatures had similar degradation shapes when plotted versus the log of the aging time. The next step is to determine whether a simple model can be used to explain the relationship between the empirically determined shift factors and the temperature. The commonly used Arrhenius functionality of eq. (2) would predict that

$$a_T = \exp\frac{E_a}{R}\left(\frac{1}{T_{ref}} - \frac{1}{T}\right) \tag{3}$$

If Arrhenius is valid, a plot of the log of the a_T values versus the inverse absolute temperature should give linear behavior. Figure 10 shows that the nitrile elongation results for a_T (the crosses on the solid line) are consistent with the Arrhenius assumption, with $E_a \sim 90$ kJ/mol, determined from the slope of the line through the results. Figure 11 shows similar plots for the a_T values used to empirically superpose the elongation results for the neoprene and CSPE jacket materials. Again, reasonable Arrhenius behavior is observed with estimated E_a values of 90 kJ/mol for the neoprene and 108 kJ/mol for the CSPE.

To make predictions below the lowest experimental temperature (64.5°C; $a_T = 1$), the normal procedure would be to extrapolate the result. As an example, the dashed line in Fig. 10 shows such an extrapolation for the nitrile data. The extrapolated a_T would be ~0.014 at around 25°C, which would imply that this material would last ~70 times longer at this temperature compared to its lifetime at 64.5°C. A refined extrapolation (solid line) based on the use of ultrasensitive oxygen consumption measurements down to room temperature [4] is also shown in this figure. This extrapolation indicates an a_T of approximately 0.02 at 25°C, predicting a room temperature lifetime ~50 times longer than at 64.5°C. Predictions based on this latter extrapolation are indicated by the top x-axis in Fig. 7.

It is important to note that, unlike the normal Arrhenius testing procedure that may use only one processed datum point from each curve, the time-temperature superposition procedure illustrated in Figs. 7-9 uses all of the raw data generated for each material. When time-temperature superposition is confirmed, strong evidence therefore exists for a constant acceleration in all of the main reactions underlying degradation.

Diffusion-limited oxidation

At equilibrium in air environments, oxygen is dissolved in polymeric materials; its concentration is given by the product of the oxygen partial pressure surrounding the material and the solubility coefficient for oxygen in the material. During oxidative aging, this oxygen will react. If the rate of reaction uses up the dissolved oxygen faster than it can be replenished by diffusion from the surrounding air atmosphere, the oxygen concentration in the interior of the material will drop, potentially leading to reduced or non-existent oxidation in these regions. The importance of such effects will depend primarily on three factors: the oxygen permeability coefficient (equal to the product of solubility and diffusivity), the rate of oxygen consumption and the material thickness [4,15,16]. It turns out that such diffusion-limited oxidation (DLO) effects are quite often observed for polymers under typical accelerated aging conditions [4,11,17]. There are many experimental methods that can be used to screen for such effects [18]. One of the most useful for elastomers is modulus profiling [19], which involves an instrument that allows the modulus to be quantitatively mapped (typical experimental scatter of ±5%) across the cross-section of a material with a resolution of approximately 50 μm. Figure 12 shows modulus profiles across the 2-mm thick nitrile rubber material after aging for various times at the four highest accelerated aging temperatures [11]. The x-axis variable, P, gives the percentage of the distance from one air-exposed surface to the opposite air-exposed surface. At the highest aging temperature of 125°C, important DLO effects cause highly heterogeneous degradation to occur. Oxidative hardening is important at the sample surface, but becomes much less important in the interior regions. As the temperature is lowered, the rate of oxygen consumption goes down faster than the oxygen permeation rate, leading to reductions in the importance of DLO. At the lowest temperature of 64.5°C, where DLO effects are no longer important, the degradation gives steady homogeneous increases in modulus [11]. Besides various experimental methods capable of monitoring DLO effects, it is now possible to theoretically model DLO and therefore estimate its importance before any accelerated aging experiments are initiated [11,15,16].

Given the importance of DLO for the aging of the nitrile material, and its complex dependence on temperature, it is perhaps surprising that the elongation results for this material display both excellent time-temperature superposition and Arrhenius behavior. This turns out to be due to a fortunate circumstance, which occurs for the elevated temperature oxidation of many elastomeric materials [11]. As shown in Fig. 12, the oxidative hardening is greatest at the sample surfaces, where the oxidation is independent of DLO effects. During tensile testing, cracks would be expected to initiate at the hardened surface. If such cracks immediately propagate through the rest of the material, the ultimate tensile elongation will be directly dependent on the true, equilibrium (non-DLO influenced) oxidation. This turns out to be the case for many but not all materials where oxidative hardening dominates the degradation. Time-temperature superposition of the surface modulus results for the nitrile material leads to shift values (the diamonds in Fig. 10) virtually identical to those found for the elongation results, consistent with this

picture. For the neoprene and CSPE cable jacketing materials, important DLO effects enter at temperatures higher than those shown in Figs. 5 and 6 [13]. These high-temperature DLO effects lead to a slight lowering of the E_a values (limited high-temperature curvature in Arrhenius plots). Since anomalous high-temperature data are not needed for predictive modeling of low-temperature lifetimes, they can safely be eliminated from any analyses.

For properties that depend upon the entire cross-section of a material, DLO effects should also be expected to lead to anomalous results. For instance, time-temperature superposition is impossible for the tensile strength of the nitrile material, because it goes up at some temperatures and down at others [11]. This is not surprising since the tensile strength at break will represent the integrated force across the entire sample cross-section, implying complex behavior due to the changing importance of DLO as the temperature drops.

The above discussions are important to keep in mind when attempting to use a degradation variable as a tool for predicting material lifetimes or remaining lifetimes. Unless DLO effects are either eliminated or quantitatively understood, it will be very difficult to have confidence in lifetime predictions derived from analyzing and modeling data potentially influenced by such effects.

Wear-out approach for predicting remaining lifetime

As mentioned above, the Wear-out approach is based on the decades-old, Palmgren-Miner concept that degradation is cumulative [2,3], and that failure is therefore considered to be the direct result of the accumulation of damage with time. Models based on this concept have been largely confined to fatigue life predictions for metals and composite materials. A typical analysis begins by assuming that fatigue damage is being induced by applying a dynamic stress level r under constant frequency, temperature, moisture content, etc. conditions [20]. In this case the damage D can be written as a function of the applied stress level r and the number of fatigue cycles, n

$$D = F(n, r) \tag{4}$$

Assuming that N_i represents the number of cycles necessary to reach failure under a given constant amplitude loading condition r_i and that the damage function D starts at 0 (where $n = 0$) and reaches unity at failure (where $n = N_i$), a simple case occurs when

$$D = F(n, r_i) = f(n / N_i) \tag{5}$$

for any value of r_i. This case is referred to as a "stress-independent damage model" since the same curve will represent the relationship between D and n/N_i independent of the value of r_i. A particularly simple case occurs when the damage is linearly related to n/N_i,

a situation shown as the solid line in Fig. 13. This line is labeled P-M, since the fatigue damage model of Palmgren and Miner assumes such linear behavior.

For most real damage parameters, damage will not accumulate linearly, implying more complex damage accumulation curves. Hypothetical examples are shown by the dashed curves labeled 1, 2, and 3 on Fig. 13. Curve 3, for instance, would represent so-called induction-time behavior, in which the damage remains relatively unchanged until just before failure, where it begins to accumulate rapidly. Whatever the shape of the damage curve, whenever a stress-independent damage model holds, the same curve (e.g., curve 3 in Fig. 13) will describe the change of the damage parameter versus n/N_i, regardless of the value of r_i.

It turns out that the presence of time-temperature superposition for thermal aging of polymers is conceptually equivalent to the so-called "stress-independent damage model" used above. Instead of the damage being described generally as a function of the stress amplitude r and the number of fatigue cycles n, the damage will be given by

$$D = F(t,T) \tag{6}$$

where the aging time t replaces n and the temperature T replaces r. With τ_i representing the time to reach failure at a given temperature T_i, the case of a "stress-independent damage model" leads to

$$D = F(t,T_i) = f(t/\tau_i) \tag{7}$$

We found above that the elongation results for thermally aged nitrile rubber (Fig. 4) led to excellent time-temperature superposition (Fig. 7). If we arbitrarily define failure of the elongation as the time required for the elongation to decrease to 20% of its original value, the data of Fig. 4 can be used to estimate values of the failure times τ_i versus temperature. The results are 700, 200, 54, 15 and 5.6 days at 64.5°C, 80°C, 95°C, 111°C and 125°C, respectively. When the elongation results at each temperature are then plotted versus t/τ_i, excellent superposition (stress-independent damage) occurs as shown in Fig. 14. This is essentially the same superposed data shown in Fig. 7, except for several minor differences. First of all, instead of a log time scale, it is plotted on a linear time scale, consistent with damage accumulation discussions. Also consistent with damage accumulation ideas, the data terminate at the failure criterion of 20% of initial elongation (the right-hand axis shows the damage function D going from 0 at the top to 1 at the bottom). Finally, the data analyzed in terms of t/τ_i result in superposed data that, from a time-temperature superposition point-of-view, have slightly different shift factors (shown on Fig. 14) from the results shown in Fig. 7. This is because truncated data (down to the failure criterion) was superposed in Fig. 14 whereas the complete data set was superposed in Fig. 7. The top axis of Fig. 14 shows the superposed time axis at 64.5°C

corresponding to the bottom t/τ_i axis, obtained from the τ_i values relative to the value of 700 days at the 64.5°C reference temperature.

Now that it is obvious that time-temperature superposition is equivalent to the concept of a stress-independent damage function, we can see that the fatigue-related lower x-axis of Fig. 13 can be replaced by an axis involving t/τ_i for thermally induced chemical degradation cases (upper x-axis in Fig. 13). In fact it is clear that the nitrile experimental elongation data given in Fig. 14 represent a degradation variable whose functional dependence on time is similar to curve 1 of Fig. 13 (in this case inverted due to the manner in which D is plotted). For the simplest situation, the degradation variable would be linearly related to time, as indicated by the solid curve labeled P-M in Fig. 13. We showed earlier (Fig. 1) that the oxidation rate for many stabilized materials is often found to be relatively constant throughout the mechanical property lifetime. This implies that the underlying degradation chemistry is also relatively constant (linear) versus time. Unfortunately, the mechanical degradation variables of typical interest (e.g., elongation, tensile strength) are usually related in a complex, non-linear manner to the underlying chemistry, implying non-linear behavior even in the presence of "linear" chemistry. Whatever the shape of the damage curve, however, whenever time-temperature superposition holds (stress-independent damage model), the same curve will describe the change of the damage parameter versus fractional degradation lifetime, regardless of the temperature (Fig. 14).

We now examine a situation where we raise the temperature T_i part way through the material's degradation from T_1 to a higher Wear-out temperature T_w, whose purpose is to complete the aging of the material (hence the name Wear-out temperature). We define t_1 as the time spent at T_1 and determine the "Wear-out" time t_w subsequently required at T_w to reach failure. For any damage parameter that gives time-temperature superposition, a reasonable assumption is that the degradation level (given by the chemical changes in the material) is identical for identical values of the damage parameter regardless of the temperature used to reach this level. For such situations, the same curve will continue to be traversed independent of when the temperature is stepped from T_1 to T_w and it is easy to see from Fig. 13 that in general

$$\frac{t_1}{\tau_1} + \frac{t_w}{\tau_w} = 1 \tag{8}$$

regardless of the shape of its damage curve versus the fractional degradation lifetime.

This relationship for a step change in temperature from T_1 to T_w (or the reverse) is plotted as the solid line in Fig. 15 (bottom x-axis and left y-axis). Defining $a_{w,1}$ as the shift factor relating the two temperatures,

$$a_{w,1} = \frac{\tau_1}{\tau_w} \tag{9}$$

and combining with eq. (8) gives

$$t_w = \frac{\tau_1 - t_1}{a_{w,1}}, \tag{10}$$

which predicts a linear relationship between t_w and t_1. This relationship can also be represented by the solid line in Fig. 15, using the upper x-axis together with the right-hand y-axis, where the time on each axis runs from 0 to the failure time. We will refer to behavior described by eq. (10) as linear Wear-out behavior to distinguish it from the Palmgren-Miner linear damage behavior (line marked P-M in Fig. 13), since the latter is not required for the former. The parameter $a_{w,1}$ can be thought of as the "acceleration factor" for the Wear-out approach.

The situation becomes more complex when time-temperature superposition is invalid. An example is shown in Fig. 16, where hypothetical data for a normalized degradation variable (e.g., tensile elongation) are plotted versus log time at temperatures T_1 and T_2. It is clear that the shapes of the degradation curves at T_1 and T_2 are different, implying that the acceleration factor relating the degradation at the two temperatures depends on the damage level. If we arbitrarily choose the failure criterion as a 90% loss in the degradation variable and replot these two curves versus their normalized aging times (aging time divided by failure time), the results are shown in Fig. 17 as the two solid curves.

Suppose Wear-out experiments are performed on this hypothetical material. We will first assume that the value of the degradation variable determines the chemical degradation state regardless of how the sample reached this state. In other words, it is assumed that the chemical makeup of the sample is equivalent, as long as the value of the degradation variable is identical. This implies that stepping of the temperature to T_2 after a certain amount of aging time at T_1 will involve a horizontal shift from the T_1 curve to the T_2 curve. As an example, if the sample was exposed to T_1 until t/τ_1 reached 0.3, then the temperature was stepped to T_2, the degradation pathway would first follow the T_1 curve, then switch horizontally to the T_2 curve as indicated by the arrows on Fig. 17. After the step, the degradation will follow the T_2 curve until failure, again as indicated by the arrows along this curve ($t_2/\tau_2 \sim 0.4$ to complete the aging). Wear-out experiments based on such behavior will result in non-linear Wear-out behavior. For the case shown (Fig. 17), where the relative degradation rate at the Wear-out temperature starts out slower but later accelerates compared to the situation at T_1, the shape of the Wear-out results will be similar to the dashed curve shown in Fig. 15. In fact, if the shapes of both curves are known and the chemical state of the material on both curves is assumed to be equivalent for equivalent values of the degradation variable, the exact shape of the Wear-out curve

can be predicted. For instance, for the hypothetical results shown on Fig. 17, we saw above that $t_1/\tau_1 = 0.3$ corresponds to $t_2/\tau_2 = 0.4$. The remainder of the predicted Wear-out curve can be determined in a similar fashion; we will do this for some real elongation data below.

A more complex situation exists if the same level of degradation at the two temperatures does not correspond to equivalent material damage (e.g., the composition of chemical degradation products is different). In this case, the degradation rate after the temperature is stepped to T_2 may not be the same at the same level of the degradation variable as for a sample aged only at T_2. An example of this so-called "interaction" effect is shown in Fig.18, where the degradation rate after the step (dashed curve) is greater than predicted in the absence of interaction. Such interaction effects will normally result in non-linear Wear-out behavior. However, in contrast to the cases described above, the shape of the Wear-out curve cannot be predicted, even when the shapes of the individual curves are known.

Applying the Wear-out approach to experimental EPDM results

Our first attempt to test the Wear-out concept involved using aged samples of the SR793B-80 EPDM o-ring material studied in Part 1 of this series [1]. As shown in Part 1, reasonable time-temperature superposition occurs for its degradation properties over the normally accessible degradation temperature range of ~155°C to 111°C. This implies similar shapes for the results when plotted versus log of the aging time. Figure 19 gives, for example, the tensile elongation results plotted versus log of the aging times. At first glance, the curves have reasonably similar shapes. However, it was also determined using measured oxygen consumption results from 160°C down to 52°C that the activation energy for oxidation changes from ~118 kJ/mol at the higher temperatures to ~82 kJ/mol at lower temperatures. The oxygen consumption rate data illustrating this effect for this EPDM material are shown in Fig. 20. Since the activation energy begins to drop around 111°C, a change in oxidation mechanism must be occurring around this temperature. Therefore, we might expect to see a change in the relative shape of the degradation curves around 111°C. A careful examination of the elongation data in Fig. 19 confirms this expectation. Although the results at 155°C, 140°C and 125°C have similar shapes, the data at 111°C appear to drop off at a somewhat slower rate. Given the above two pieces of evidence for a change in mechanism occurring around 111°C, we decided to use samples from the 111°C series and from the 125°C series and test the Wear-out approach by completing the aging of these samples at 150°C.

Since 150°C and 125°C fall into the temperature region (155°C to 125°C) where excellent evidence for time-temperature superposition exists, we would expect linear behavior for the Wear-out results on the 125°C samples. Assuming that 50% absolute elongation corresponds to "failure", we find from the 125°C elongation plot that failure occurs after ~158 days. At 150°C (dashed line on Fig. 19 resulting from interpolating

between the 140°C and 155°C curves), failure takes ~20.5 days. Therefore, the predicted Wear-out behavior (T_w = 150°C) for the samples previously aged at 125°C would be given by the straight line in Fig. 21 connecting 158 days on the x-axis with 20.5 days on the y-axis. On the other hand, since the 111°C elongation results change shape relative to the higher temperature results, we would expect non-linear Wear-out results for samples previously aged at 111°C. If no interactions occur (the value of the degradation variable determines the chemical degradation state regardless of how the sample achieved this state), we can use the shapes of the elongation results at 111°C and 150°C to predict the shape of the Wear-out data. Using the same failure criterion of 50% absolute elongation, this procedure leads to the solid curve on Fig. 22.

Since we showed in Part 1 [1] that oxidation of this material (oxygen consumption) correlates with elongation, surface modulus, density and solvent uptake, it is possible to use any of these parameters to follow the degradation at the Wear-out temperature (150°C). Actual practice, however, necessitates monitoring the degradation parameter versus time so the time required to reach the selected failure value can be determined. Elongation was not used since it is a destructive technique and would therefore require a large amount of material. Solvent uptake measurements were not considered because they are moderately time-consuming and require a fair amount of material (especially since they should be considered destructive). The best parameters are probably surface modulus and density, since both are essentially non-destructive (if necessary repeated measurements can be made on a single sample) and require only small sample sizes. In addition, both parameters show dramatic induction-time behavior (similar to curve 3 of Fig. 13), implying that the point of failure should be relatively easy to determine. For our initial screening studies, we chose to follow only the density, and selected 1.16 g/cc as the failure point (this value of density corresponded to elongation reaching ~50%- see Table 3 of Reference [1]). Figure 23 shows density results versus 150°C aging time for samples that had previously been aged for the indicated number of days at 125°C. The values of t_w required at 150°C for the density to reach 1.16 g/cc are plotted as squares versus the aging times at 125°C in Fig. 21. The experimental results are reasonably linear and are in good agreement with the solid theoretical line predicted from the elongation behavior, offering the first piece of evidence for the potential of the Wear-out approach. Density results versus 150°C aging time for the 111°C pre-aged samples are shown in Fig. 24; values of t_w obtained from these curves are plotted as squares in Fig. 22. Although the experimental results are somewhat higher than the theoretical expectations for short 111°C aging times and somewhat below theoretical expectations at longer 111°C aging times, their overall behavior is in reasonable accord with theory. Given the experimental scatter in the elongation and density results, the level of agreement is in fact encouraging.

A better method of analyzing the Wear-out results of Figs. 23 and 24 involves a procedure that we define as "time-degradation superposition", in which the Wear-out density curves are shifted to a reference state with an additive shift factor defined as a_D.

When density Wear-out results are available for initially unaged material, these data (the right-hand curves in Figs. 23 and 24) are selected as the reference state ($a_D = 0$). If interactions are absent during the Wear-out exposures, the shapes (on a linear time plot) of the degradation curves during the high temperature (150°C) exposures should be identical. This is obvious from Fig. 17, where the lack of interactions implies that regardless of the preaging time on the T_1 curve, all of the degradation curves for subsequent aging at T_2 (the Wear-out temperature) will superpose when translated horizontally to the T_2 curve. When interactions are present, it is clear from Fig. 18 that such superposition will not occur. Thus by attempting time-degradation superposition, we are able to test for the importance of interaction effects. In addition, this procedure uses all of the Wear-out data instead of just a single processed point (e.g., the time required to reach a density of 1.16 g/cc).

Figures 25 and 26 show the results obtained from applying the time-degradation superposition procedure to the data of Figs. 23 and 24, respectively. The empirically derived additive shift factors (designated as a_D) that led to the best superposition are indicated in Figs. 25 and 26, where the reference condition ($a_D = 0$) corresponds to the previously unaged material. For both sets of data the superposition is reasonable and offers evidence that important interaction effects are absent for the experimental conditions studied. The tremendous advantage of the time-degradation superposition approach is that a defined failure criterion is not required. In order to use the shift factors for predicting remaining lifetime, however, a failure criterion must obviously be selected. If, for instance, we again select 1.16 g/cc as the failure criterion, the superposed results of Figs. 25 and 26 indicate that 21 d at 150°C is required to reach this condition for the previously unaged material. With this failure criterion, a plot of 21 - a_D versus aging time at 125°C and 111°C would represent a Wear-out plot that is equivalent to the failure time plots of Figs. 21 and 22, respectively. The distinction would be that the experimental data come from time-degradation superposition (all of the data used) instead of from single processed points (the estimated failure times). The results of this procedure are plotted as crosses on Figs. 21 and 22. The excellent agreement between the crosses and the squares is not surprising given the observation of reasonable time-degradation superposition.

Applying the Wear-out approach to Surveillance EPDM o-rings

The main goal of the Wear-out approach is to predict the remaining lifetime of a material that has been aging for extended periods of time at ambient conditions. An example is the application of such techniques to surveillance weapon materials in order to estimate remaining lifetimes in ambient weapon environments. In such cases, the initial aging temperature T_1 would represent ambient weapon conditions and T_w an elevated Wear-out temperature. It is easy to see from the general discussion and the experimental results above that linear Wear-out results will not always occur. However, applying the Wear-out method for predicting remaining life involves periodically generating Wear-out results on ambiently aged material as a function of time under ambient conditions. Early

results would allow initial estimates of remaining life by assuming linear extrapolation behavior. As more data became available, more refined and confident extrapolations could be made.

An important consideration in choosing the Wear-out temperature (T_w) for such experiments is minimizing the temperature difference between the ambient temperature and T_w. This is obvious for several reasons. First and foremost, the likelihood for acceptable time-temperature superposition of the degradation variables and therefore reasonably linear Wear-out behavior, is increased if the temperature difference is minimized, since a larger temperature difference increases the chance for a change in the chemical degradation mechanism. In addition, keeping T_w as low as possible reduces the chances of physical complications such as diffusion-limited oxidation effects. Opposing the desire to keep T_w as low as practical is the need to complete the Wear-out experiments in a reasonable time period. Balancing these two contradictory requirements leads to the conclusion that T_w should be selected such that degradation is completed over a few weeks to a few months time frame.

As an example of using the Wear-out approach on materials aged for extended periods of time, we were able to acquire EPDM o-rings from a weapon that had been aged for ~23 years in the field. These o-rings were originally obtained from Parker Seal Group and were designated E529-60. Since Parker still supplies this compound, we purchased new E529-60 o-rings and used these as baseline materials for our Wear-out experiments. For o-ring degradation, the property of most interest is the decay in the sealing force. Earlier studies on the similar SR793B-80 EPDM material showed that the point where significant loss of sealing force occurred was correlated to the point of significant loss of the more-easily measured tensile elongation as well as the point at which other properties (density, modulus) begin to show significant increases [1]. Based on the known aging behavior of the SR793B-80 EPDM material [1], we decided that a T_w of 140°C would yield convenient Wear-out times (up to several months). With this in mind, we first carried out aging of the new material at 140°C to determine how the tensile elongation and density behave at this temperature. The elongation results, shown in Fig. 27, indicate that it takes ~70 days to reach a reasonable failure criterion of 40% absolute elongation (10% of initial). As anticipated [1], the density results (squares in Fig. 28) begin to show significant increases at about the same time. Since we had a limited amount of the 23 year-old EPDM material, only density measurements could be used for the Wear-out experiments. The density results for the 23 year-old material versus aging time at the Wear-out temperature of 140°C are plotted as the crosses in Fig. 28. Because the aged material results have shifted a very small amount relative to the unaged results, it is immediately clear that very little degradation has occurred after 23 years. If we arbitrarily select 1.24 g/cc density as a measure of failure (corresponds to elongation dropping to ~10% of initial), it takes ~70 days for the unaged material to reach 1.24 g/cc versus ~65 days for the aged. The Wear-out plot of these data, shown in Fig. 29, leads to an initial lifetime estimate of ~320 years. This initial estimate is very approximate given the small differences found between the newly purchased and 23 year-old materials and

the expectations of data scatter for the same material purchased 25 years apart. At this point, all we can confidently say is that a very long lifetime is indicated by the results. This prediction of a long lifetime is consistent with the accelerated aging predictions for the earlier SR793B-80 EPDM reported in Part 1 [1].

By periodically obtaining additional ambiently aged samples of increasing age, future Wear-out experiments can be used to generate more data for Fig. 29, leading to refined and more confident lifetime estimates. Of course, by definition, we do not have the complete degradation curve under ambient conditions. Therefore we do not have explicit evidence that the ambient degradation would time-temperature superpose with degradation at the Wear-out temperature, a forecaster of linear Wear-out behavior. In fact, we will never have such evidence in the absence of the complete ambient data up to failure. But, if we have confirmed time-temperature superposition from careful accelerated experiments, there would be a reasonable chance that this superposition will remain valid down to ambient conditions. This implies that Wear-out experiments on the long-term, ambiently aged samples could give reasonably linear behavior. The key is that Wear-out experiments versus ambient aging time will allow us to check the linearity of the results and whether the predicted failure time from extrapolation of the Wear-out data is consistent with the failure time predicted from extrapolation of the conventional accelerated aging results.

It is important to note that it is not necessary to obtain an unaged sample in order to make remaining lifetime predictions, as long as real-time aged samples of differing ages are available to allow the shape of the Wear-out plot to be followed and extrapolated. This is significant since it may not always be possible to obtain an unaged sample 15 or 20 years after the material of interest is placed into use. This observation, in fact, constitutes another advantage of the Wear-out approach relative to other lifetime prediction methods.

Notice also, that to utilize the Wear-out approach, we do not have to explicitly know how the damage parameter depends on time at a constant temperature. It could have linear Palmgren-Miner dependence or any other shape, such as the three example curves in Fig. 13. If we have unaged material to evaluate, experiments on this material at the Wear-out temperature will allow us to determine the shape of the damage parameter versus time at the Wear-out temperature. The shape could of course be the same or different under low temperature ambient conditions dependent upon whether time-temperature superposition holds. An interesting situation occurs if a degradation parameter can be found that appears to follow linear P-M behavior under accelerated conditions. In this case, simply following the degradation parameter versus field aging time may also yield linear results assuming time-temperature superposition is valid down to ambient conditions. If the observed linearity under ambient conditions is assumed to continue till failure, simply following the degradation parameter and extrapolating its values to its failure value offers a direct method of predicting remaining lifetime. Full-scale Wear-out experiments like those described above would not be necessary in this situation.

Unfortunately, it is rather unusual to find linear Palmgren-Miner behavior for polymer degradation parameters. Although most studies have examined degradation behavior under laboratory (accelerated) conditions, if linear behavior was observed under such conditions, there would be a reasonable chance (if time-temperature superposition holds) that similar linear behavior would occur at ambient temperatures. We showed above that density for EPDM materials tends to follow "induction time" behavior (Curve 3 of Fig. 13). For other materials, density sometimes gives reasonably linear behavior. For example, density measurements on the nitrile rubber material studied earlier (Figs. 4, 7 and 12) are reasonably linear over the mechanical property lifetime. This is seen from superposed macroscopic density results taken at 64.5°C and 80°C (Fig. 30), temperatures that are only slightly influenced by diffusion-limited oxidation anomalies (Fig. 12). For this material, the relatively linear behavior of density is consistent with the observation that the isothermal oxygen consumption rates are relatively constant versus aging time (Figs. 1 and 2). Linear density behavior has also been observed for thermal aging of a PVC cable jacketing material at 110°C [21]. On the other hand, induction-time behavior similar to that found for the EPDM materials has been observed from density measurements for additional EPDM materials and for crosslinked polyolefin and chlorosulfonated polyethylene materials [21].

Another degradation parameter that occasionally shows linear or near-linear behavior is the oxygen induction time (OIT). In pioneering work, Kramer and Koppelmann [22] utilized custom, highly sensitive DTA sensors to isothermally measure the time before significant oxidation begins (the OIT) for polybutylene after aging for various times at 150°C. Figure 31 shows that the OIT results measured at 180°C are linearly related to the 150°C aging times. Other examples of reasonably linear OIT behavior are found [23]. On the other hand, similar to the situation observed for density and elongation, much of the OIT literature shows that this degradation parameter does not follow linear P-M behavior. For instance, Kramer, et. al. [24] found moderate curvature for OIT measurements taken on the same polybutylene material as that studied in Fig. 31 but for different aging and OIT measurement temperatures (Fig. 32). In OIT studies of an oven-aged, stabilized polyethylene material, Matsumoto [25] found first order decay of the OIT, implying an exponential decay with time. Anandakumaran et. al. [26,27] observed very non-linear, complex behavior for the oven aging of several XLPE and EPR cable insulation materials. Figure 33 shows some of their results for two of these materials.

It is important to note that, even when such complex, non-linear time-dependence occurs for a degradation parameter, the Wear-out approach will still be applicable and may give linear results. For example, assume that the time dependence of OIT under ambient temperature conditions was the same as the complex time dependence for EPR at 140°C shown in Fig. 33. In this case, Wear-out aging at 140°C (using periodic OIT measurements till a failure criterion is reached) of ambiently aged samples would be predicted to result in linear Wear-out plots. In addition, time-degradation superposition of the OIT Wear-out results would be expected to have a superposed shape similar to the complex shape found for the EPR aging at 140°C.

REFERENCES

1. K. T. Gillen, M. Celina, R. L. Clough, G. M. Malone, M. R. Keenan and J. Wise, "New Methods for Predicting Lifetimes in Weapons. Part 1- Ultrasensitive Oxygen Consumption Measurements to Predict the Lifetime of EPDM O-Rings", Sandia National Laboratories Report SAND98-1942, (September 1998).
2. A. Palmgren, Z. Vereins Deutscher Ingenieure, 68, 339 (1924).
3. M. A. Miner, J. of Appl. Mech., A159 (1945).
4. J. Wise, K. T. Gillen and R. L. Clough, Polym. Deg. Stab. 49, 403 (1995).
5. ASTM Standard D792-91- Density and Specific Gravity of Plastics by Displacement.
6. M. Celina, K. T. Gillen, J. Wise and R. L. Clough, Radiat. Phys. Chem., 48, 613 (1996).
7. T. Kelen, **Polymer Degradation**, Van Nostrand Reinhold, 1983.
8. J. L. Bolland, Proc. R. Soc. London, A186, 218 (1946).
9. L. Bateman, Q. Rev. (London), 8, 147 (1954).
10. K. T. Gillen, M. Celina, R. L. Clough and J. Wise, Trends in Polym. Sci., 5, 250 (1997).
11. J. Wise, K. T. Gillen and R. L. Clough, Polymer, 38, 1929 (1997).
12. K. T. Gillen and R. L. Clough, Polym. Degrad. & Stab., 24, 137 (1989).
13. K. T. Gillen, R. L. Clough, M. Celina, J. Wise and G. M. Malone, Proceedings of the 23rd Water Reactor Safety Information Meeting, NUREG/CP-0149, Vol. 3, p. 133 (1995).
14. J. D. Ferry, **Viscoelastic Properties of Polymers**, John Wiley and Sons, 1970.
15. A. V. Cunliffe and A. Davis, Polym. Deg. Stab., 4, 17 (1982).
16. K. T. Gillen and R. L. Clough, Polymer, 33, 4358 (1992).
17. R. L. Clough and K. T. Gillen, Polym. Deg. Stab., 38, 47 (1992).
18. K. T. Gillen and R. L. Clough, **Handbook of Polymer Science and Technology,** Vol. 2, N. P. Cheremisinoff, Ed., Marcel Dekker, 1989, Ch. 6.
19. K. T. Gillen, R. L. Clough and C. A. Quintana, Polym. Degrad. & Stabil., 17, 31 (1987).
20. W. Hwang and K. S. Han, J. Composite Mater., 20, 125 (1986).
21. K. T. Gillen, M. Celina and R. L. Clough, Radiat. Phys. Chem., 56, 429 (1999).
22. E. Kramer and J. Koppelmann, Polym. Deg. Stab., 14, 333 (1986).
23. L. R. Mason and A. B. Reynolds, "Reduction of Oxidation Induction Time Testing to Practice as a Life Assessment Technique for Cable Insulation", EPRI Report EPRI TR-106370 (March 1996).
24. E. Kramer, J. Koppelmann and J. Dobrowsky, Die Angew. Makromol. Chemie, 158/159, 187 (1988).
25. S. Matsumoto, J. Polym. Sci., P. C. Ed., 21, 557 (1983).
26. K. Anandakumaran and D. J. Stonkus, Polym. Eng. Sci., 32, 1386 (1992).
27. K. Anandakumaran, et. al., "Improved Conventional Testing of Power Plant Cables", EPRI Report EPRI TR-105581 (September 1985).

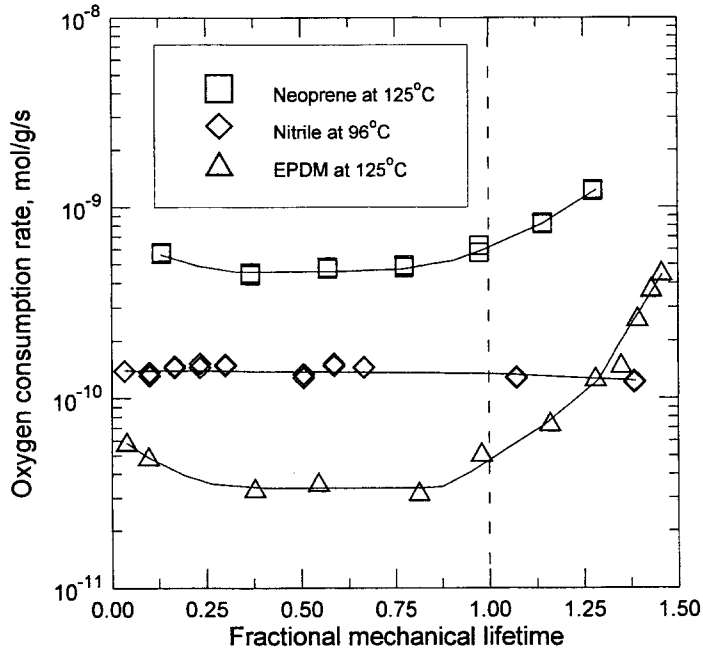

Figure 1. Oxygen consumption rates for the indicated materials and temperatures. For each condition, the results are plotted versus the fractional mechanical property lifetime, which is defined as the aging time divided by the time required for the ultimate tensile elongation to reach 10% of its unaged value.

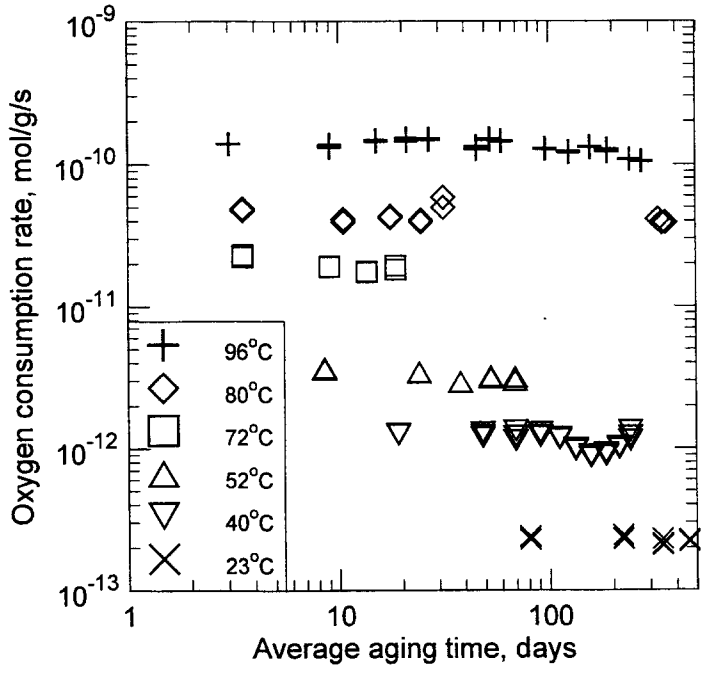

Figure 2. Oxygen consumption rates for a nitrile rubber material versus aging time at the indicated temperatures.

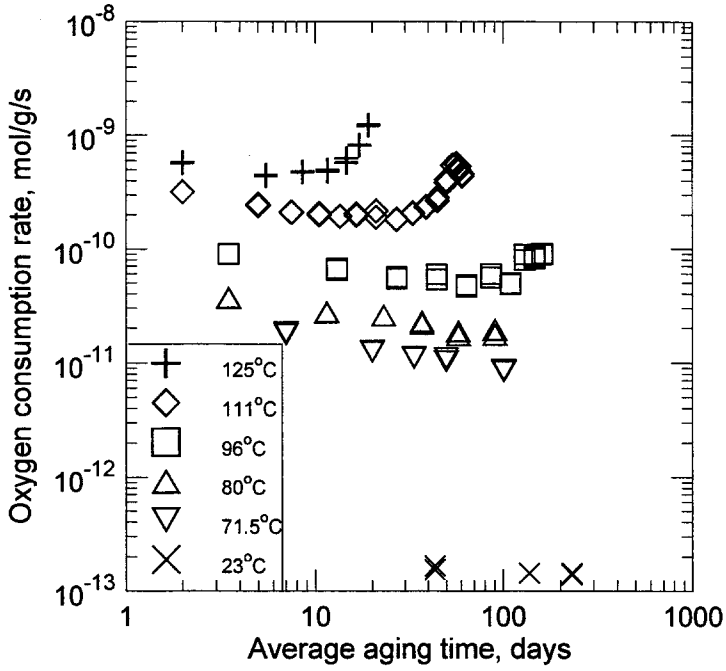

Figure 3. Oxygen consumption rates for a neoprene rubber material versus aging time at the indicated temperatures.

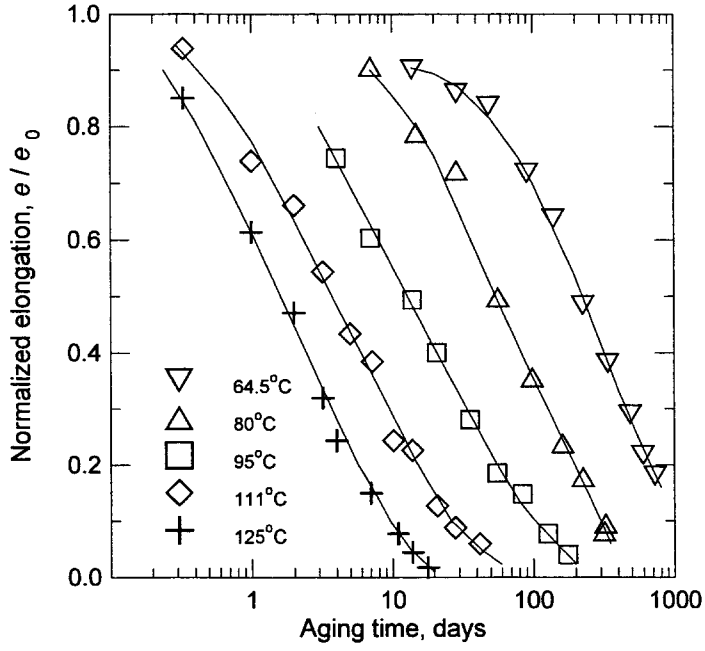

Figure 4. Normalized elongation results for the nitrile rubber versus aging time at the indicated temperatures.

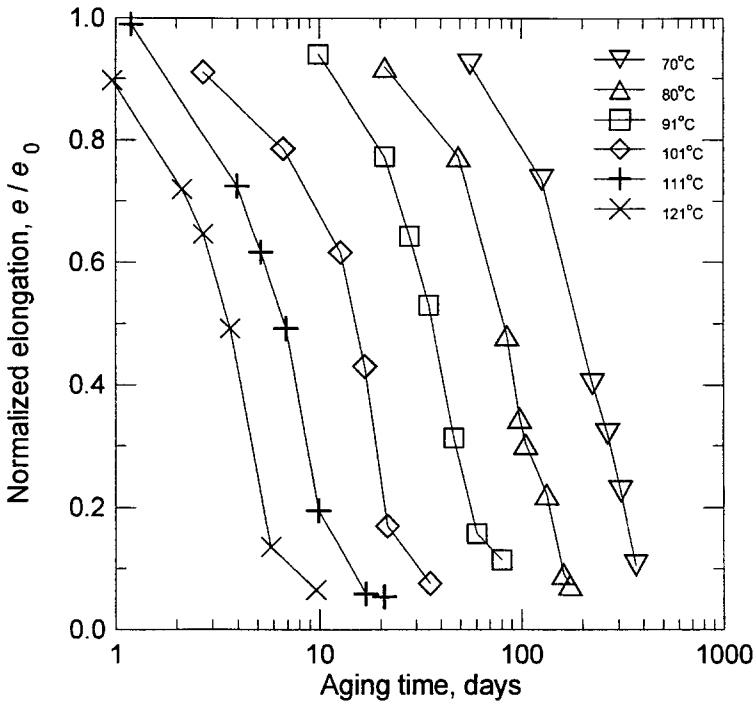

Figure 5. Normalized elongation results for a neoprene cable jacketing material versus aging time at the indicated temperatures.

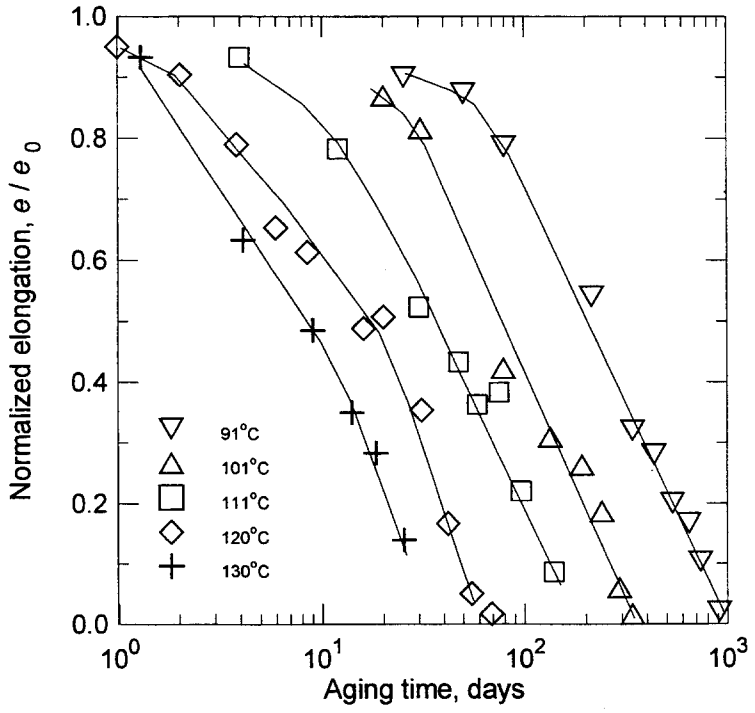

Figure 6. Normalized elongation results for a chlorosulfonated polyethylene (CSPE) cable jacketing material versus aging time at the indicated temperatures.

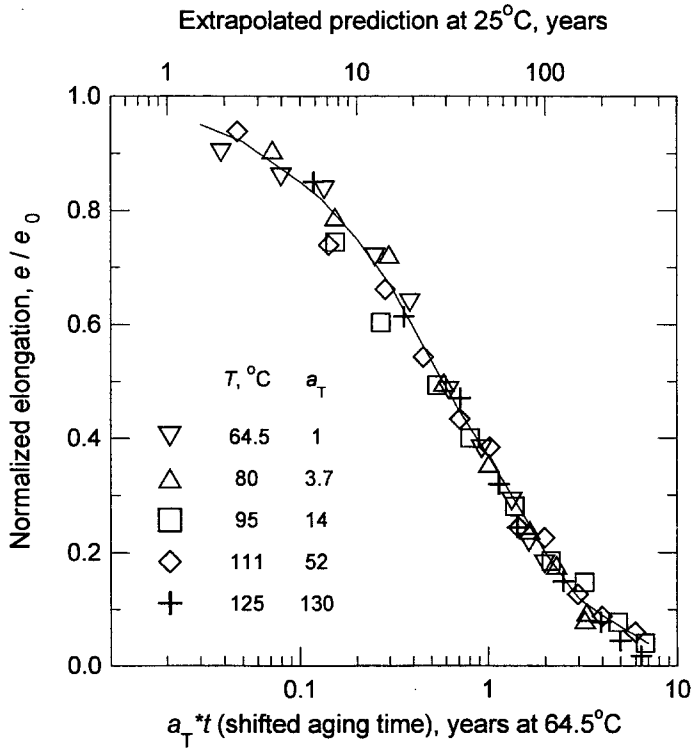

Figure 7. Empirical time-temperature superposition of the nitrile data from Fig. 4 at a reference temperature of 64.5°C (lower x-axis). The upper x-axis shows predictions resulting from an extrapolation of the 64.5°C superposed results to 25°C.

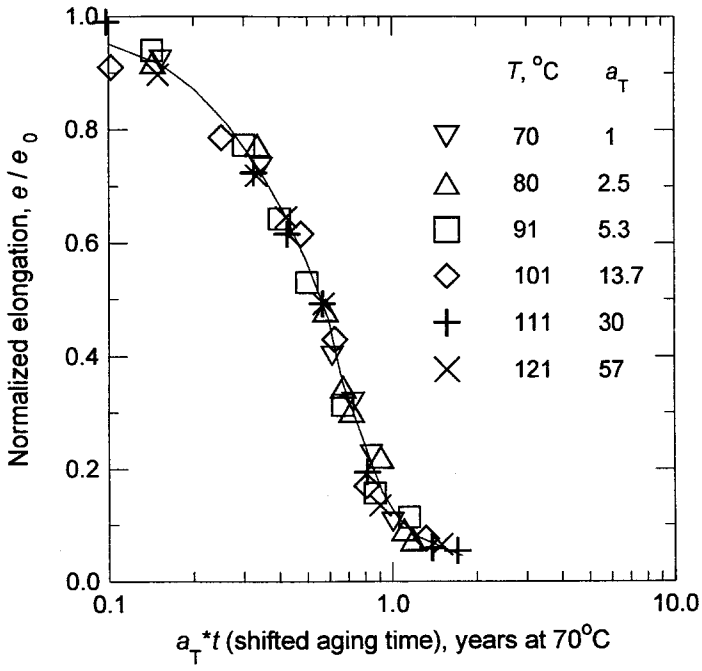

Figure 8. Empirical time-temperature superposition of the neoprene data from Fig. 5 at a reference temperature of 70°C.

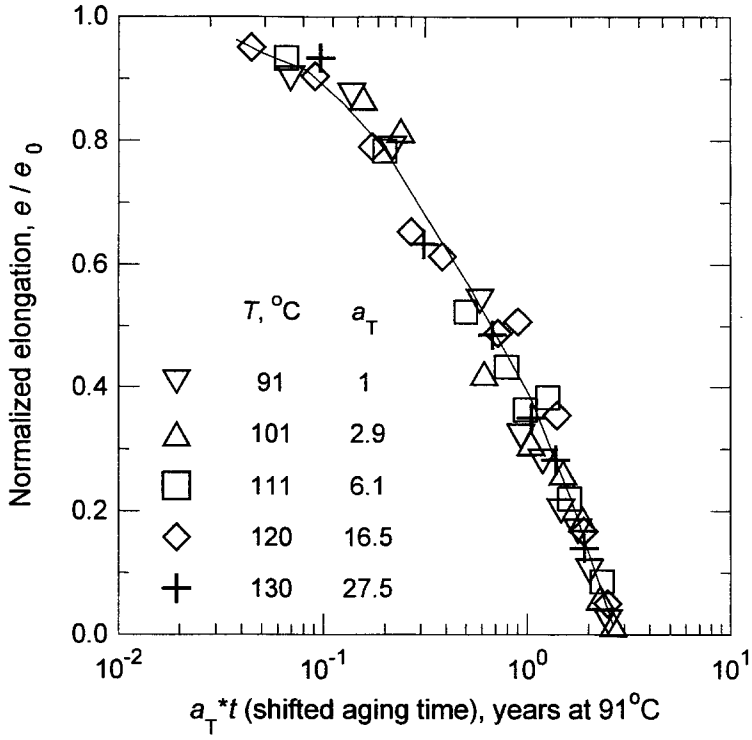

Figure 9. Empirical time-temperature superposition of the CSPE data from Fig. 6 at a reference temperature of 91°C.

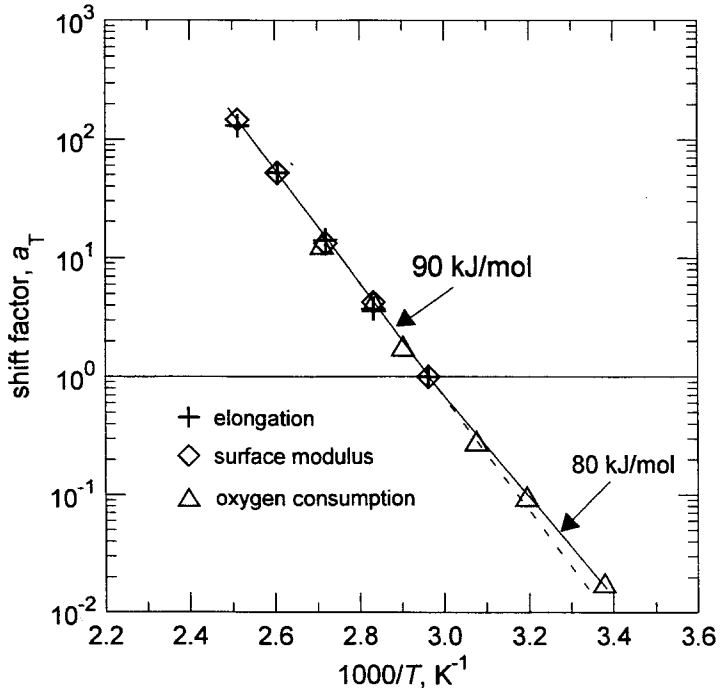

Figure 10. Arrhenius plot of shift factors obtained from empirical time-temperature superposition of the indicated nitrile rubber degradation parameters.

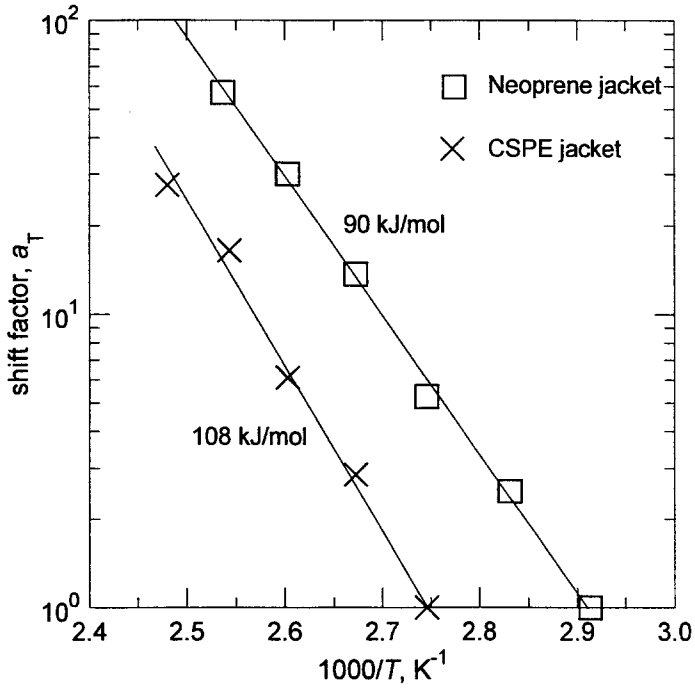

Figure 11. Arrhenius plots of the empirical shift factors used to generate the time-temperature superposed elongation results for the neoprene (Fig. 8) and the CSPE (Fig. 9) cable jacketing materials.

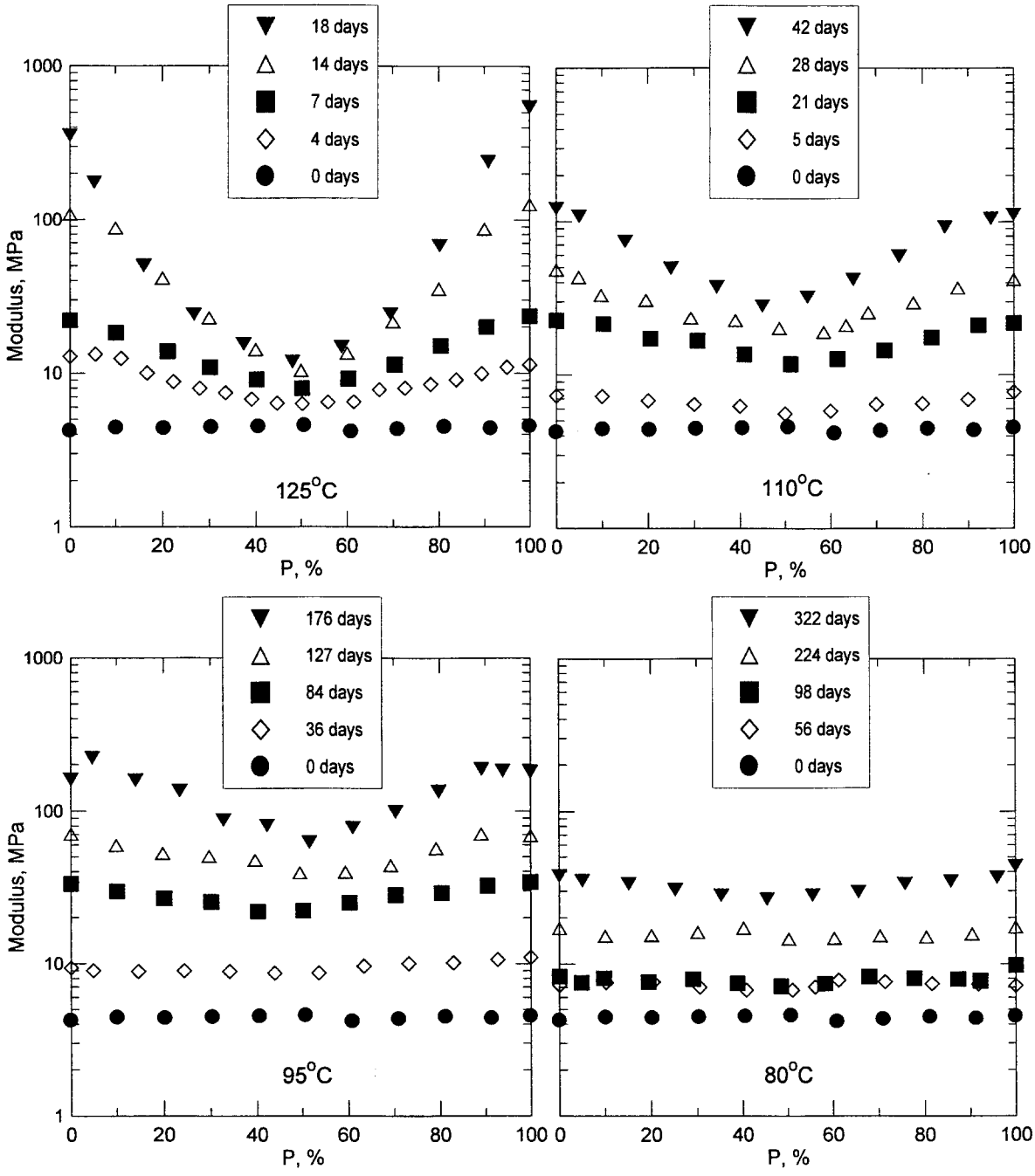

Figure 12. Modulus profiles versus aging time and temperature for the 2-mm thick nitrile rubber. P denotes the percentage of the distance from one air-exposed sample surface to the opposite air-exposed surface.

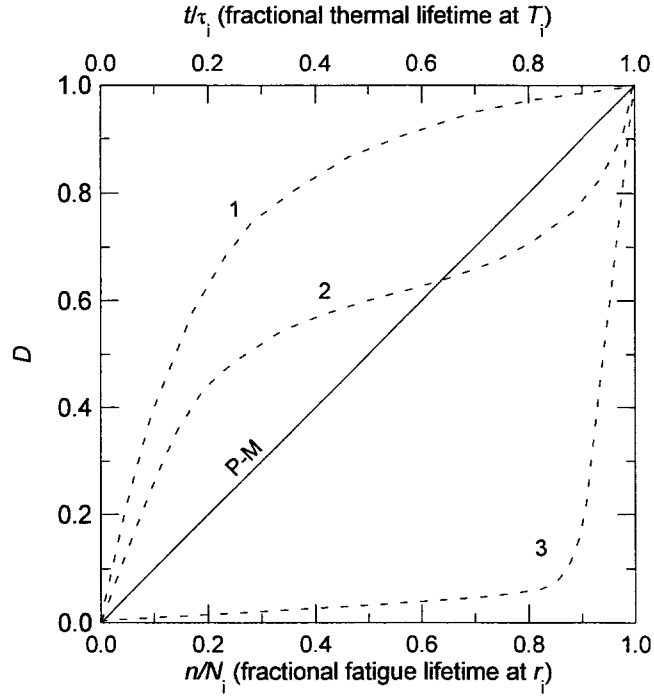

Figure 13. Schematic showing some representative relationships between degradation parameters and fractional fatigue lifetime (lower x-axis) or, equivalently, fractional thermal lifetime (upper x-axis).

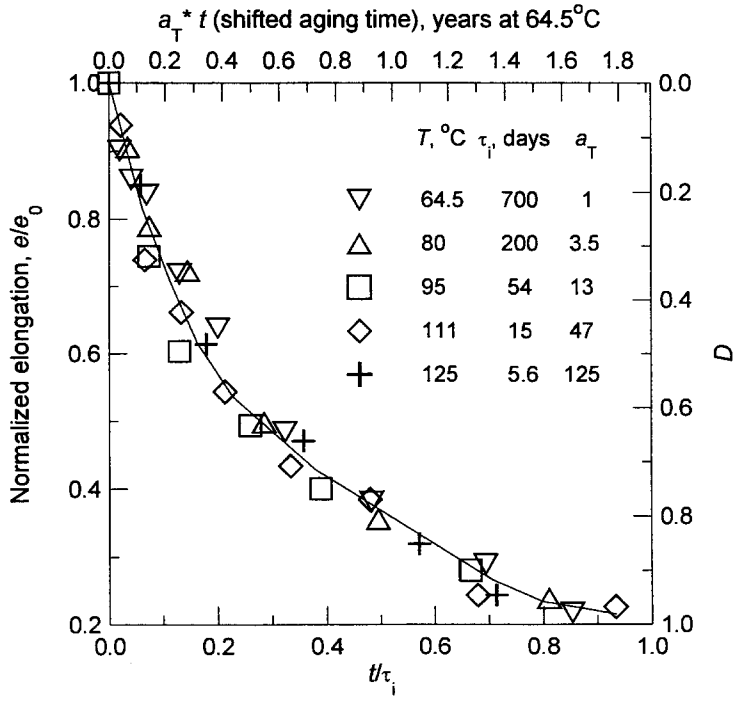

Figure 14. Normalized elongation results for the nitrile rubber material (left y-axis) versus fractional thermal lifetime (lower x-axis) for the indicated temperatures. The right y-axis shows the degradation variable, whereas the top x-axis shows the time-temperature superposed data at a reference temperature of 64.5°C.

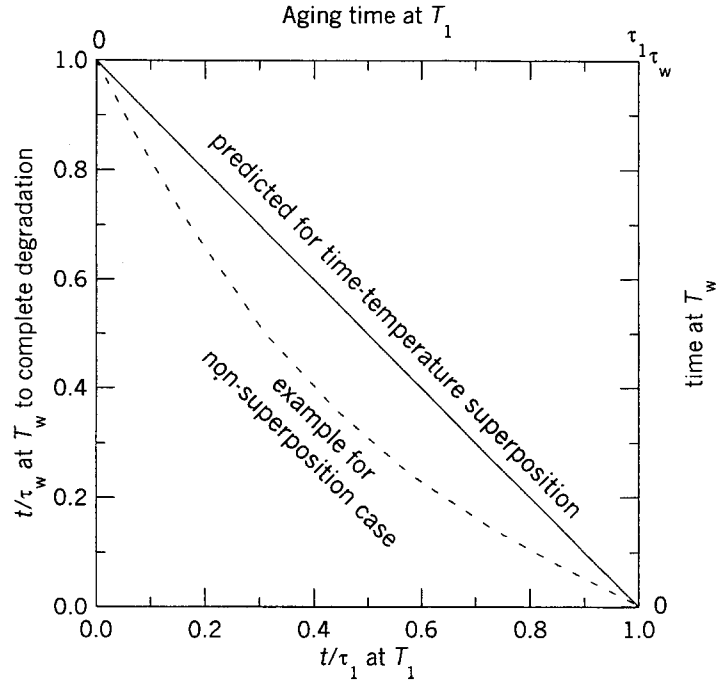

Figure 15. Hypothetical Wear-out plots showing predictions when time-temperature superposition is valid (solid line) and an example when superposition is invalid (dashed curve).

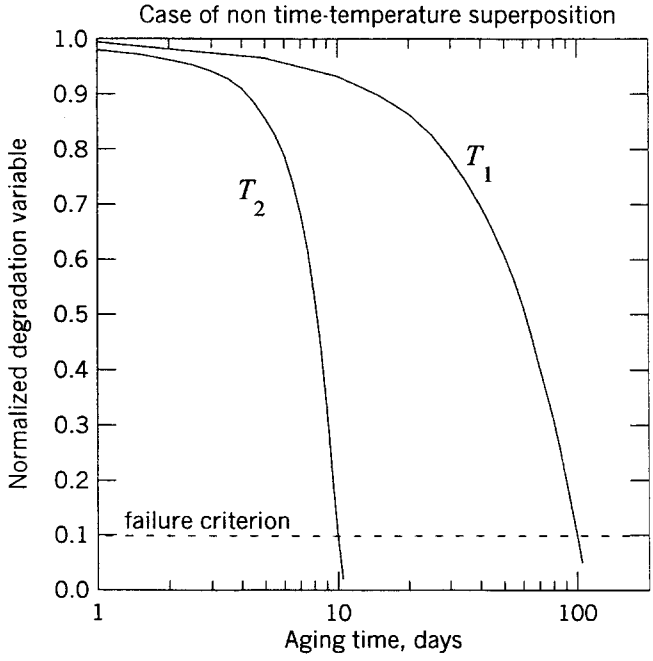

Figure 16. Hypothetical example of a degradation property that does not time-temperature superpose.

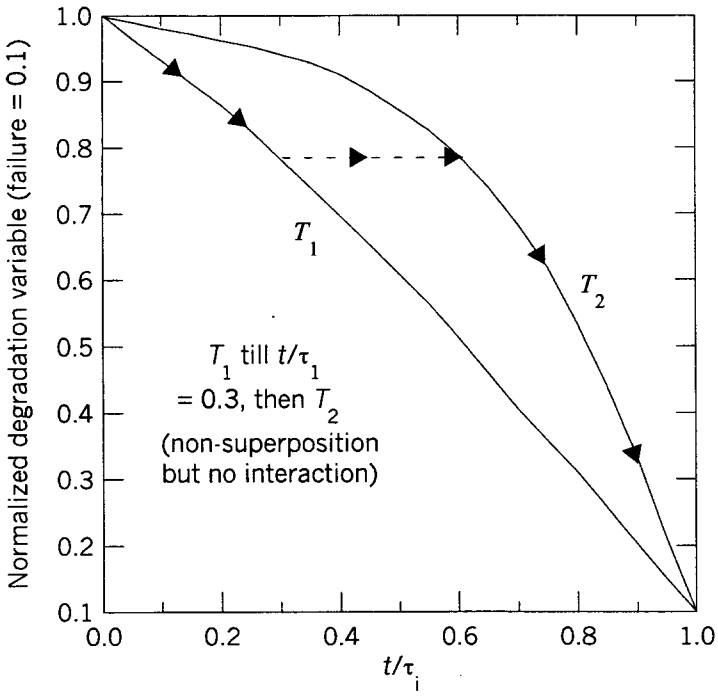

Figure 17. The non-superposable results from Fig. 16 plotted against fractional thermal lifetime. A hypothetical Wear-out experiment is shown by the arrows assuming no interaction.

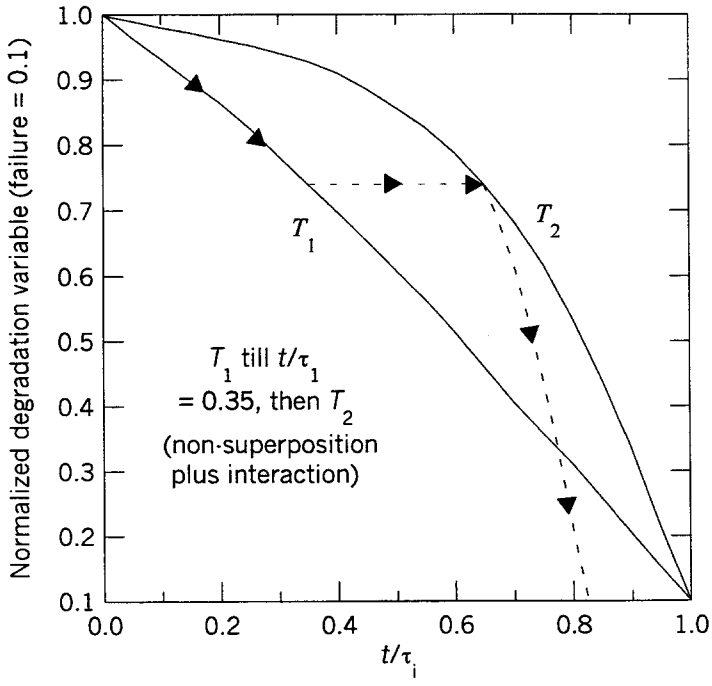

Figure 18. The non-superposable results from Fig. 16 plotted against fractional lifetime. A hypothetical Wear-out experiment is shown by the arrows assuming interaction.

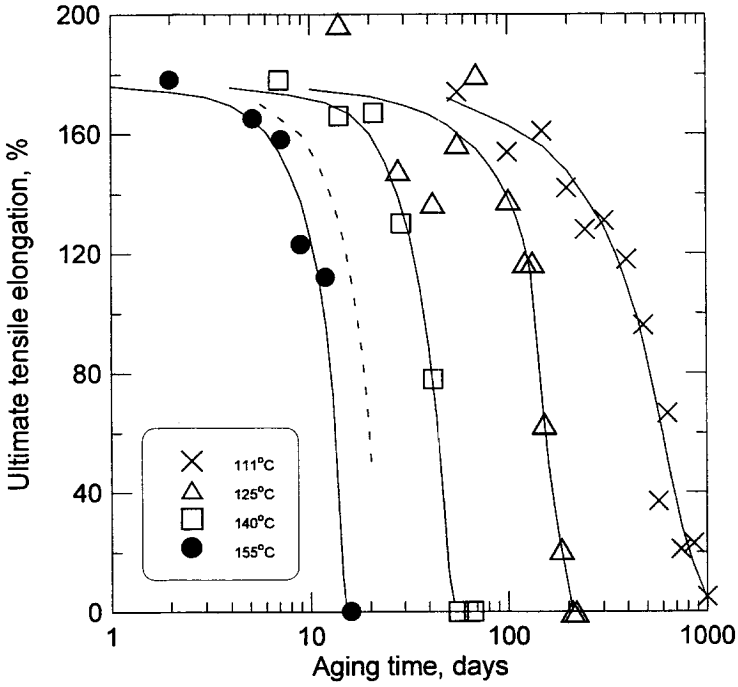

Figure 19. Elongation results versus time and temperature for the SR793B-80 EPDM material [1].

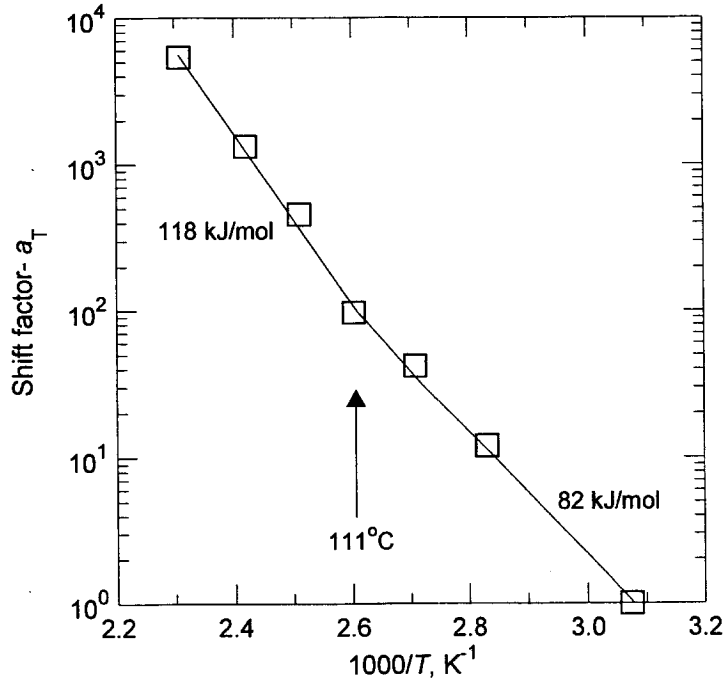

Figure 20. Oxygen consumption rate measurements versus inverse absolute temperature for the SR-793B EPDM material.

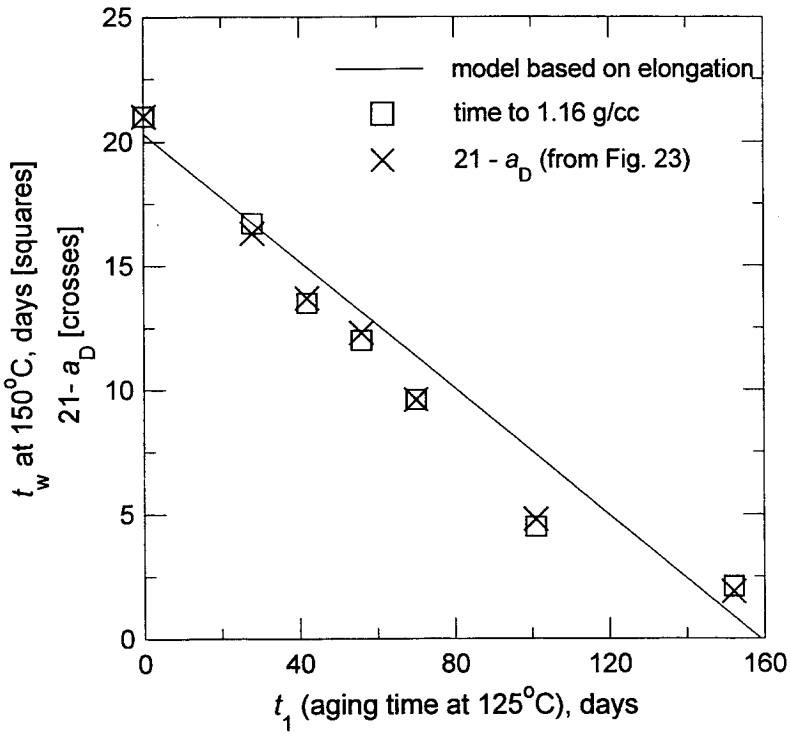

Figure 21. Theoretical and experimental Wear-out results for the SR793B-80 EPDM material for aging at 125°C.

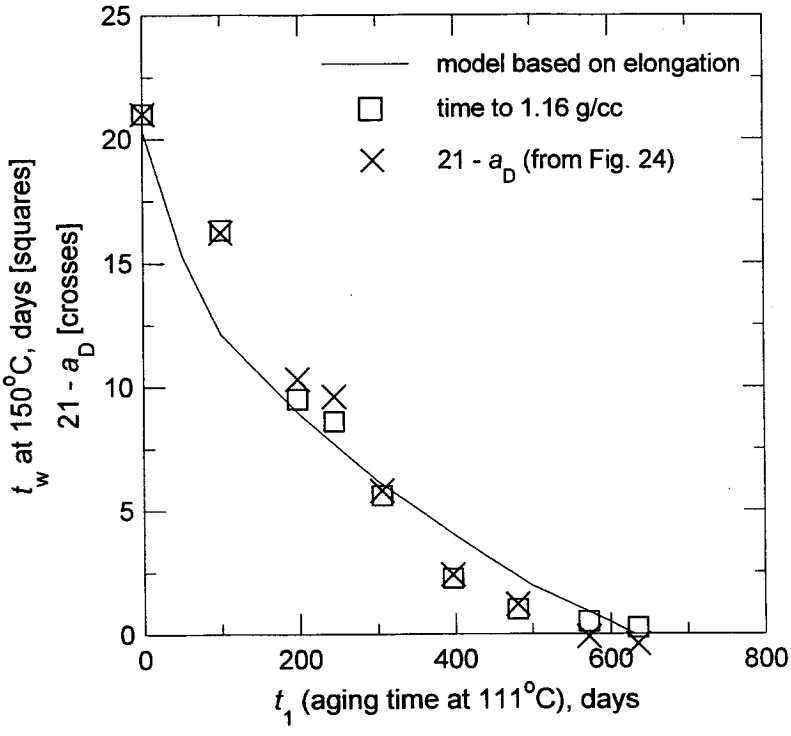

Figure 22. Theoretical and experimental Wear-out results for the SR793B-80 EPDM material for aging at 111°C.

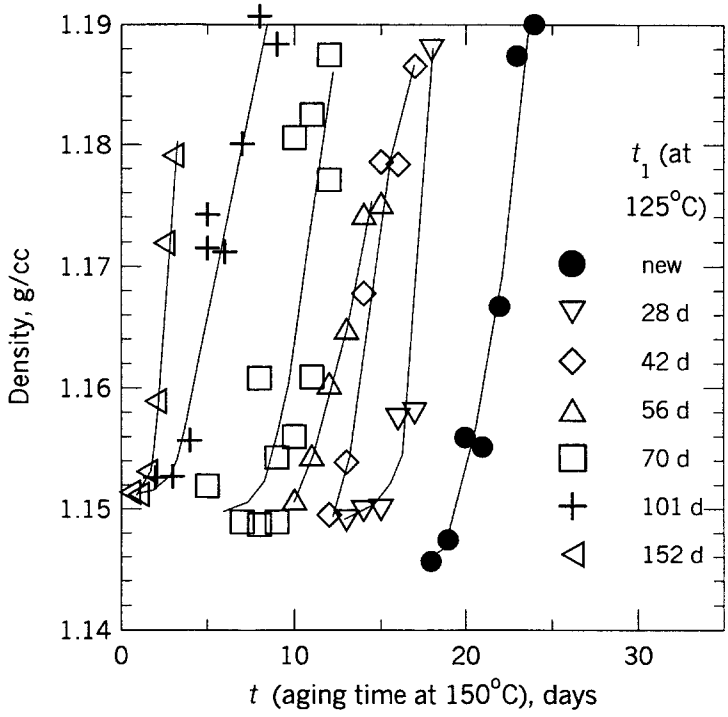

Figure 23. Density results versus aging time at 150°C for the SR793B-80 EPDM samples previously aged at 125°C for the indicated times.

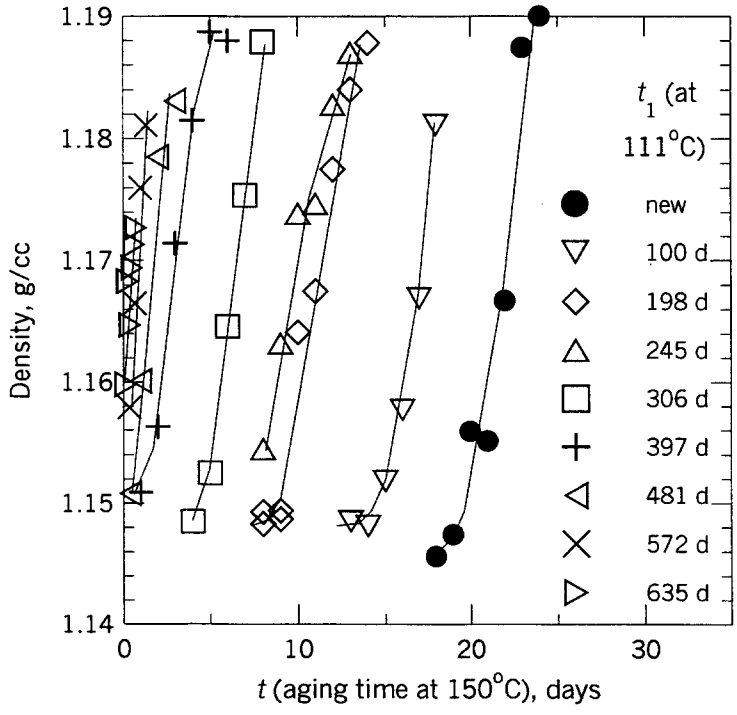

Figure 24. Density results versus aging time at 150°C for the SR793B-80 EPDM samples previously aged at 111°C for the indicated times.

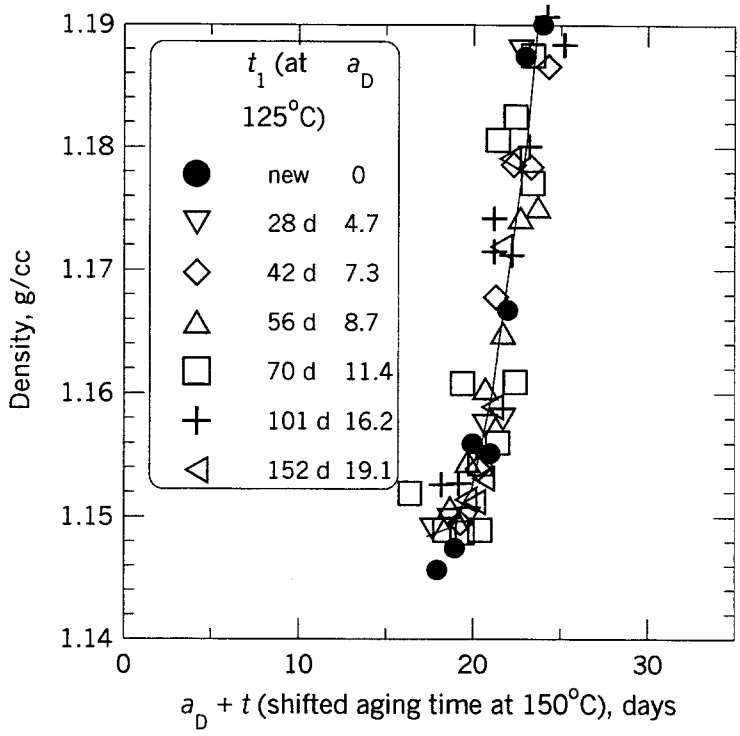

Figure 25. Time-degradation superposition of the density results shown on Fig. 23.

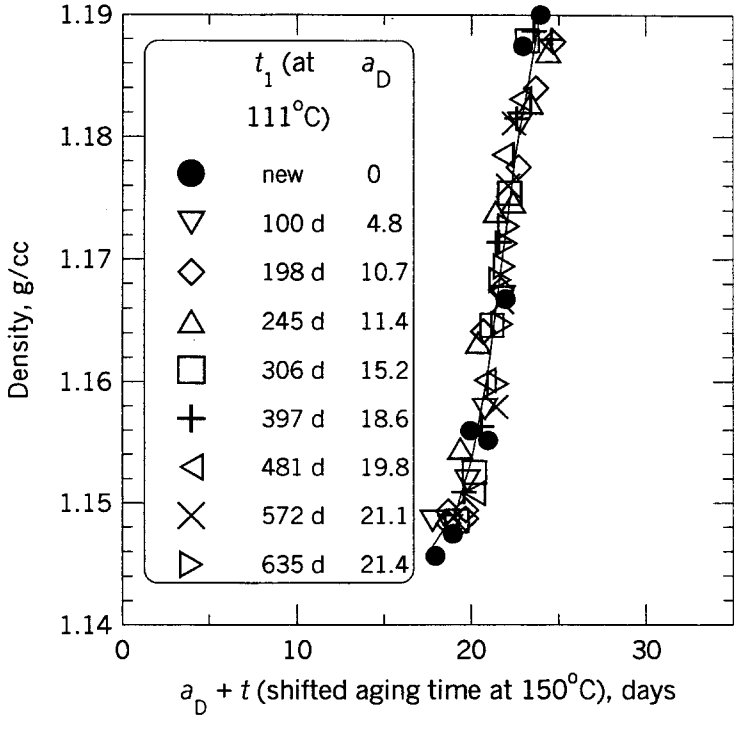

Figure 26. Time-degradation superposition of the density results shown on Fig. 24.

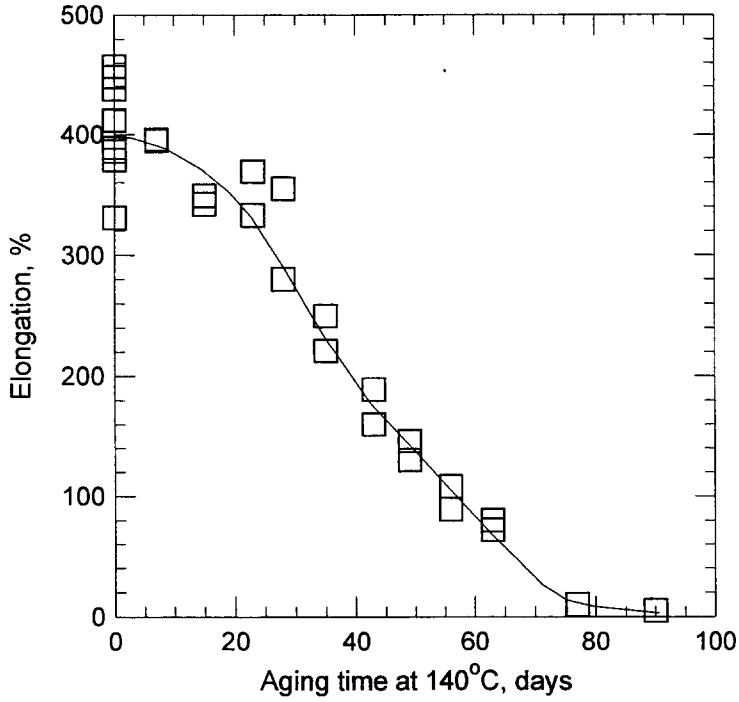

Figure 27. Elongation results versus aging time at 140°C for the Parker E529-60 EPDM o-rings.

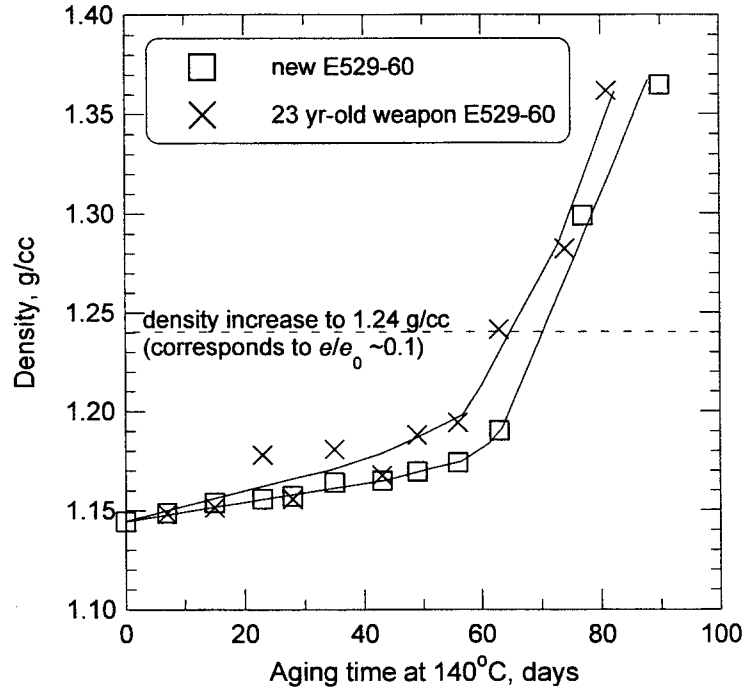

Figure 28. Density results versus aging time at 140°C for new Parker E529-60 EPDM o-rings and for EPDM o-rings aged for 23 years in the field.

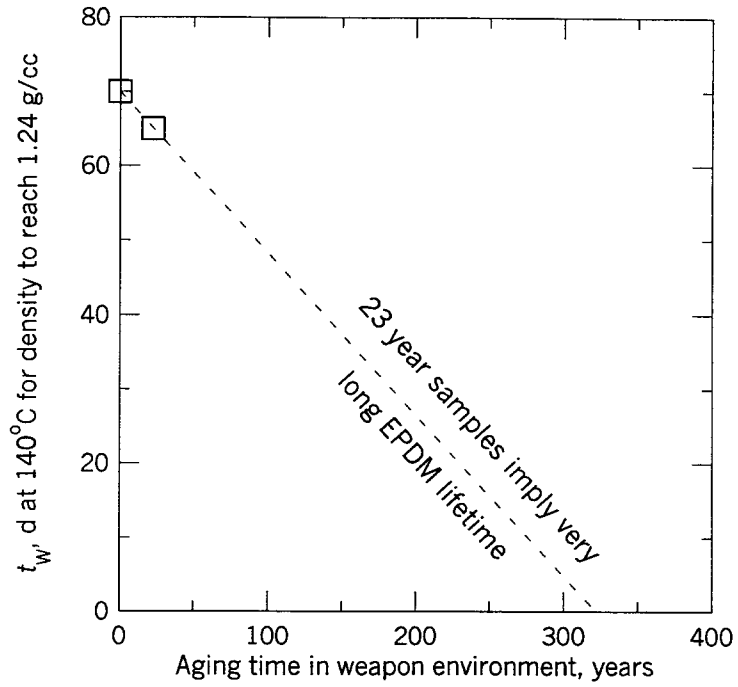

Figure 29. Wear-out plot using the density results of Fig. 28.

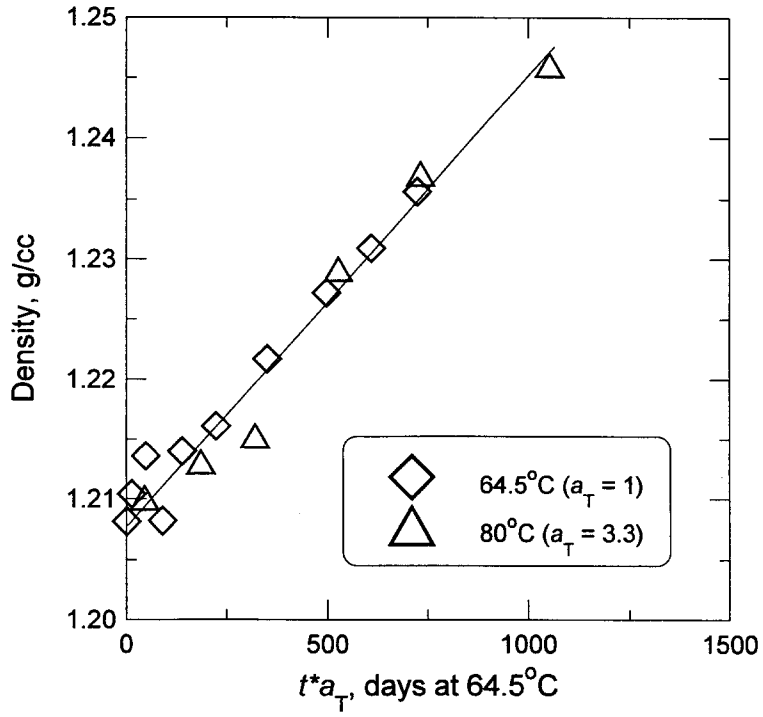

Figure 30. Time-temperature superposed density results for the nitrile rubber material at a reference temperature of 64.5°C.

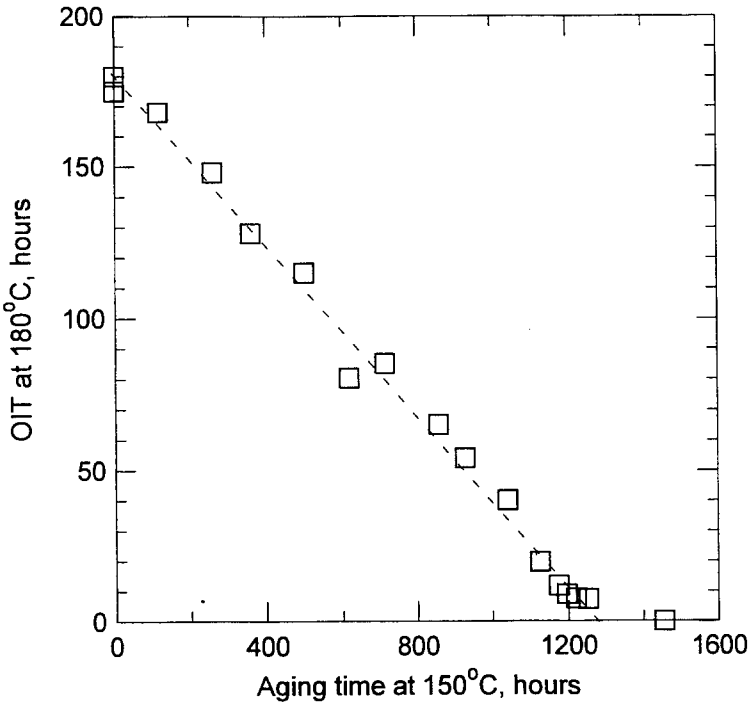

Figure 31. OIT results for polybutylene versus aging time at 150°C from reference 22.

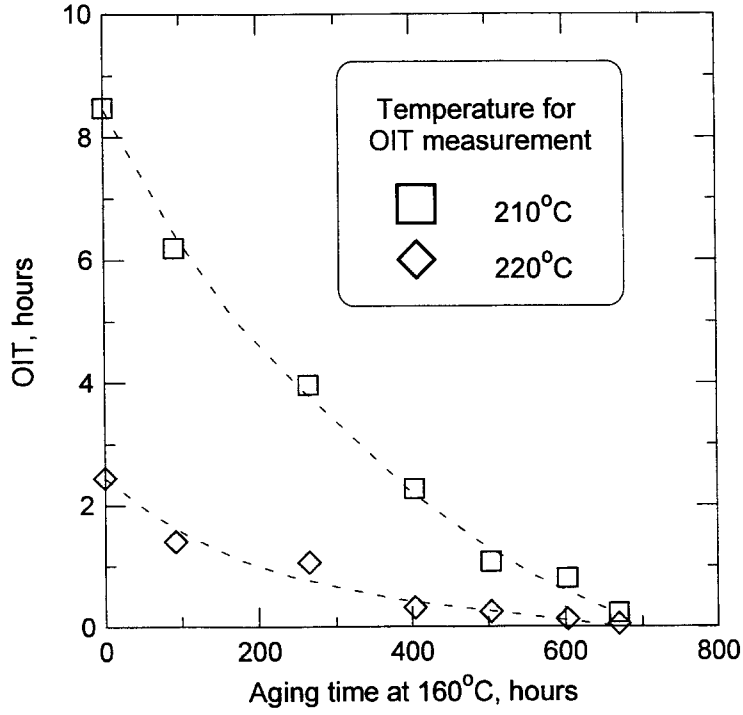

Figure 32. OIT results for polybutylene versus aging time at 160°C from reference 24.

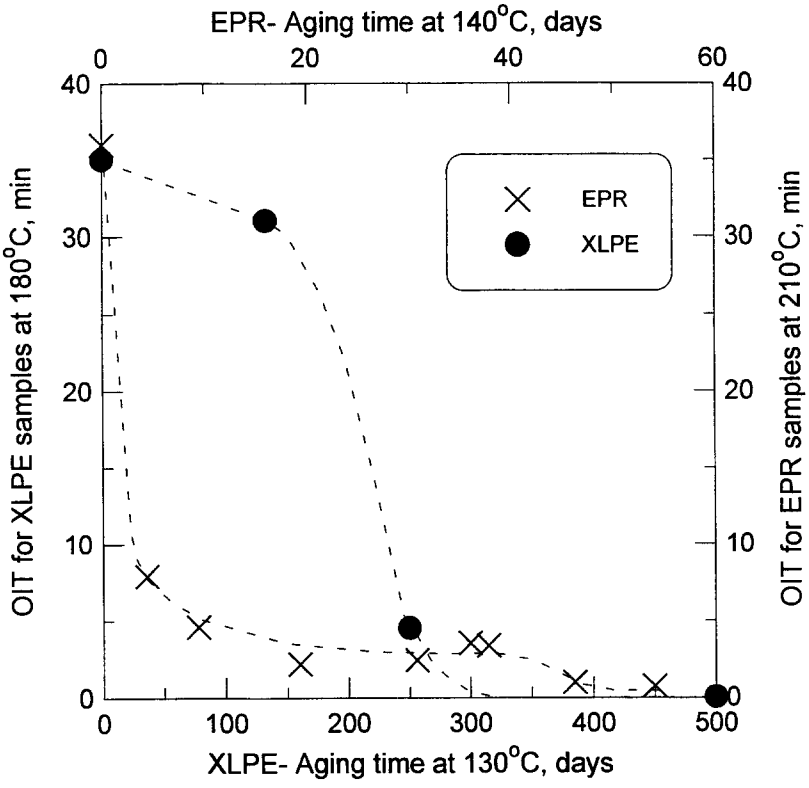

Figure 33. OIT results for XLPE versus aging time at 130°C (left y-axis, bottom x-axis) and OIT results for EPR versus aging time at 140°C (right y-axis, top x-axis)- from references 26 and 27.

Eric Cochran, DP-22
U. S. Department of Energy
Forrestal
Washington, DC 20585

Jim Lemay
Lawrence Livermore National Laboratory
P. O. Box 808, Mail Stop L-322
Livermore, CA 94550

Mark Wilson
AlliedSignal
Federal Manufacturing & Technologies Division
Attn: M. H. Wilson, 834-2C43
P.O. Box 419159
Kansas City, MO 64141-6159

Phil Holtzman
Strategic Technology and Resources
195 High Street
Winchester, MA 01890

Dennis Harrison
U. S. Department of Energy
19901 Germantown Road
Germantown, MD 20874-1290

Duli Agarwal
U. S. Department of Energy
19901 Germantown Road
Germantown, MD 20874-1290

Jit Vora
U. S. NRC
11545 Rockville Pike
N. Bethesda, MD 20852-2738

Bob Lofaro
Brookhaven National Laboratories
Associated Universities
Building 130 Upton, L. I., NY 11973

Tom Doyle
Pacific-Sierra Research Corporation
1400 Key Boulevard, Suite 700
Arlington, Virginia 22209

John E. Hutchinson
Plant Support Engineering
Nuclear Power Group
Electric Power Research Institute
1300 Harris Blvd.
Charlotte, NC 28262

Gary Toman
Plant Support Engineering
Nuclear Power Group
Electric Power Research Institute
1300 Harris Blvd.
Charlotte, NC 28262

Sandia- Internal

1	MS 9006	C. L. Knapp (2220)
4	MS 0367	R. J. Salzbrenner (1835)
1	MS 0475	R. C. Hartwig (2105)
1	MS 1393	A. J. West (2200)
1	MS 0639	R. W. Lizut (12303)
1	MS 0479	R. D. Holt (2151)
1	MS 0447	P. D. Hoover (2111)
1	MS 0479	R. S. Pacheco (2165)
1	MS 0447	A. L. Hillhouse (2111)
1	MS 0847	D. J. Segalman (9124)
1	MS-0847	C. S. Lo (9123)
1	MS 9403	J. C. Wang (8723)
1	MS 9402	L. A. Domeier (8722)
1	MS 9042	W. Lu (8725)
1	MS 9042	V. Revelli (8727)
1	MS 9405	R. Jones (8726)
1	MS 1435	A. K. Hays (1800)
1	MS 1407	R. A. Assink (1811)
5	MS 1407	M. Celina (1811)
1	MS 1407	R. L. Clough (1811)
10	MS 1407	K. T. Gillen (1811)
1	MS 0343	M. R. Keenan (1812)
1	MS 0783	J. M. Clauss (5854)
1	MS 0742	J. R. Guth (6401)

1	MS 0744	D. L. Berry (6420)
1	MS 0746	D. G. Robinson (6411)
1	MS 9018	Central Technical Files (8940-2)
2	MS 0899	Technical Library (4916)
1	MS 0612	Review and Approval Desk (4912) For DOE/OSTI